Revision 1 (6849R)

Crystallographic and Textural Evidence for Precipitation of Rutile, Ilmenite, Corundum, and Apatite Lamellae From Garnet

Duncan S. Keller* & Jay J. Ague

Department of Geology and Geophysics
Yale University
PO Box 208109
New Haven, CT 06520-8109 USA
*Corresponding author: duncan.keller@yale.edu

ABSTRACT

Garnet is a common metamorphic and igneous mineral with extensive solid solution that can be stable to mantle depths ≥400 km. High-*T* and/or high-*P* garnet may contain oriented lamellae of other minerals, most commonly simple oxides (e.g. rutile, ilmenite), apatite and, in ultrahigh-*P* cases, silicates including pyroxene and amphibole. Lamellae have classically been considered to be precipitation features preserving a record of former garnet chemistry richer in the lamellae nutrients (e.g. Ti^{4+}). Such microtextural origins in precipitation systems (e.g. alloys) have long been studied via the crystallographic orientation relationships (COR) that form between a host and a separating phase, and by the shape-preferred orientation (SPO) of the lamellae. Recently, however, alternative hypotheses to precipitation have been suggested that require emplacement of lamellae in garnet by fluids, or co-growth, overgrowth, or inheritance mechanisms. These hypotheses posit that lamellae cannot be used to study former garnet chemistry. Moreover, they predict that lamellae phases, SPO, and COR should differ widely between localities, as lamellae formation will be controlled by a variety of local rock-specific factors such as fluid presence, fluid chemistry, or mineral growth sequence. On the other hand, if lamellae characteristics are largely consistent between localities, it likely reflects control by precipitation energetics, rather than external factors. There have been few comparative COR studies in geologic systems, but integrative assessment of COR, SPO, and lamellae assemblages should fingerprint lamellae growth process. To test the precipitation and alternative hypotheses, we collected large electron backscatter diffraction (EBSD) datasets for rutile, ilmenite, and apatite lamellae in garnet from the Brimfield Schist, Connecticut (≥1,000 °C metamorphism; Central Maine Terrane, U.S.A.). We analyzed these data alongside published EBSD data for rutile, ilmenite, and corundum from metapegmatites metamorphosed in the eclogite facies from the Austrian Alps (Griffiths et al.

2016). The apatite dataset is the first of its kind, and reveals that apatite preferentially aligns its close-packed direction parallel to that of garnet (*c-axis*$_{\text{apatite}}$//<111>$_{\text{garnet}}$). We also recognize a rutile-garnet COR related to those in meteorites with Widmanstätten patterns which are unequivocal products of exsolution. This is the first identification of direct similarities between silicate-oxide and metal-metal COR of which we are aware. Significantly, this rutile-garnet COR is found in diverse geologic settings including Connecticut and Idaho (USA), Austria, Germany, Greece, and China over a broad range of bulk-rock compositions. Results for all lamellae minerals show that COR are largely consistent between localities and, furthermore, are shared between apatite, ilmenite, and corundum. Moreover, between 70% and 95% of lamellae have COR and there is a dominant COR for each lamellae phase. Calculations show that *d-spacing* ratios of host/lamellae pairs can successfully predict the most commonly observed specific COR (those COR with two or more axial alignments with the host). These results, especially similarity of COR from markedly different geologic settings and a low diversity of lamellae minerals, are fully consistent with lamellae formation by precipitation (likely via exsolution). In contrast, the alternative hypotheses remain unsupported by COR results as well as by mineralogical and petrological evidence. Lamellae with similar traits as those in this work should thus be considered precipitates formed during unmixing of garnet compositions originally stable at elevated or extreme pressures and temperatures.

Keywords: Garnet, Rutile, Ilmenite, Corundum, Apatite, crystallographic orientation relationship, precipitation, Widmanstätten pattern

INTRODUCTION

Networks of oriented lamellae are commonly considered to have precipitated from the host phase with shape-preferred orientation (SPO) controlled at least in part by the symmetry of the host (Putnis 1992) (Fig. 1). Exsolution is one form of precipitation that is widely recognized in mineralogy. Precipitated lamellae typically have rational crystallographic orientation relationships (COR) with their host, controlled by minimization of volume free energy, surface energy, and/or strain energy during precipitation (e.g. Nabarro 1940; Fisher et al. 1952; Putnis 1992; Hwang et al. 2016; Habler and Griffiths 2017). COR have been characterized for many host-precipitate pairs, and multiple COR exist for some pairs (e.g. Bunge et al. 2003; Morito et al. 2006; Habler and Griffiths 2017). Moreover, different host-lamellae pairs can have the same COR (Griffiths et al. 2016). These relationships have been valuable for inferring lamellae growth processes (e.g. Stanford and Bate 2005; Wenk et al. 2011; Proyer et al. 2013; Hwang et al. 2016).

There are many well-documented examples of precipitation in Earth and planetary sciences, including Widmanstätten patterns (Thomson structures) in meteorites (Goldstein and Ogilvie 1965, Bunge et al. 2003, Cayron 2014) (Fig. 1a) as well as spinodal decomposition lamellae and exsolution lamellae in feldspars (Putnis, 1992; Muñoz et al. 2016). Each example shares the same prominent characteristic of an ordered 3-dimensional distribution of lamellae throughout the host, although lamellae need not have sharp edges and may occur on the sub-micron scale as in the case for perthitic alkali feldspar.

Aluminum-silicate garnet ($X^{2+}{}_3Y^{3+}{}_2Si_3O_{12}$, isometric), notable for its wide stability across planetary pressures (*P*) and temperatures (*T*), may contain oriented lamellae of other minerals such as rutile (α-TiO_2, tetragonal), ilmenite ($FeTiO_3$, trigonal), and/or apatite [$Ca_5(PO_4)_3(F,Cl,OH)$, hexagonal] (Fig. 1b-e). Garnets with oxide lamellae are reported from kimberlites (e.g. Griffin et al. 1971); high pressure and ultrahigh-pressure rocks (e.g. van Roermund and Drury 1998; Zhang and Liou 1999; Wang et al. 1999; van Roermund et al. 2000; Ye et al. 2000; Dobrzhinetskaya et al. 2004; Spengler et al. 2006; Hwang et al. 2007; Griffin 2008; Zhang et al. 2011; Proyer et al. 2013; Wood et al. 2013); ultrahigh-temperature rocks and high-pressure granulites (e.g. O'Brien 2008; Liu et al. 2010; Ague et al. 2013; Axler and Ague 2015a; Keller and Ague 2018); rocks from tectonic sequences with eclogites and other high-pressure rocks (Griffiths et al. 2016); and, very rarely, amphibolite-facies rocks (e.g. Hwang et al. 2015). Apatite lamellae are found in garnet from high-pressure and ultrahigh-pressure rocks (Fung and Haggerty 1995; Ye et al. 2000; Mposkos and Kostopoulos 2001; Perchuck 2008; Ruiz-Cruz and Sanz de Galdeano 2013; Alifirova et al. 2015; Axler and Ague 2015; Sakamaki et al. 2016; Keller and Ague 2018).

At these elevated or extreme *P*-*T* conditions, trace constituents including Ti, P, and Na may be soluble in garnet (Ringwood and Major 1971; Ono 1998; Song et al. 2005; Hermann and Spandler 2008; Zhang et al. 2011; Ague and Eckert 2012; Konzett 2016; Ackerson et al. 2017a). For example, experimental work has shown that garnets stable in the granulite and eclogite facies may contain >1 wt% TiO_2 (e.g. Auzanneau et al. 2009; Qian and Hermann 2013; Ackerson et al. 2017a). Consequently, a growing number of studies interpret lamellae as arising from expulsion, during cooling or decompression, of trace substitutions stable at peak *P*-*T* conditions in garnet (e.g. van Roermund and Drury 1998; Zhang and Liou 1999; van Roermund et al. 2000; Ye et al. 2000; Dobrzhinetskaya et al. 2004; Spengler et al. 2006; Zhang et al. 2011; Ague et al. 2013; Proyer et al. 2013; Alifirova et al. 2015; Axler and Ague 2015a). In addition, coupled majorite-type substitutions involving Si on the garnet octahedral site (Y^{3+} in formula above), such as $2Al^{3+} = Si^{4+}+M^{2+}$, typify garnet stable at $P > \sim5$ GPa (M^{2+} = divalent cation, e.g. Ca, Fe, Mg). These substitutions, which also commonly involve Ti, P, and Na, can be used to identify samples returned from upper mantle settings (e.g. Ringwood and Major 1971; Sobolev and Lavrent'ev 1971; Hermann and Spandler 2008; Harte 2010; Wood et al. 2013; Wijbrans et al. 2016).

A significant complication, however, is that rocks returned slowly from (ultra)high temperature crustal or mantle conditions commonly re-equilibrate during transport, leaving retrogressed garnet chemistries due to rapid diffusion (Chakraborty and Ganguly 1992; Chu and Ague 2015). On the other hand, if lamellae precipitate they can be armored by refractory, mechanically-robust garnet, thus providing valuable clues to the original garnet chemistry that can illuminate prior conditions. This includes identification of (ultra)high-temperature and (ultra)high-pressure rocks, even those from as deep as >300 km within Earth (van Roermund and Drury 1998; Ye et al. 2000; Dobrzhinetskaya et al. 2004; Griffin 2008; Zhang et al. 2011), and for studying Earth's mantle chemistry in garnet-bearing lithologies. Moreover, lamellae would provide a record of precursor garnet compositions for any grade of metamorphism following which they precipitate, with (precursor) garnet chemistry potentially distinguishing between, for example, ultrahigh-temperature garnet and high-pressure garnet.

Strong evidence for precipitation of rutile, ilmenite, and apatite has been discovered in the form of: (1) Ti and/or P chemical depletion halos surrounding lamellae in garnet (Ague and Eckert, 2012; Axler and Ague 2015a) and (2) garnet-oxide COR (Proyer et al. 2013; Griffiths et al. 2016; Xu and Wu 2017). The presence of COR alone may not be enough to demonstrate a precipitation origin, as COR may form in a number of different ways. Thus, some controversy persists regarding COR and lamellae formation processes, with alternatives to precipitation such as co-growth with garnet or deposition by infiltrating fluids proposed (e.g. Wang 1999; Hwang et al. 2007). Notably, however, there is disagreement about whether these processes are even able to generate lamellae or COR (Proyer et al. 2013). Furthermore, no mineralogical studies have yet produced definitive evidence that a given COR between the same host-lamellae pair can form by significantly different processes, such as precipitation, emplacement, or replacement. This strongly suggests that if COR can be produced in experimental work or correlated across materials, they will be useful for diagnosing textural formation processes.

High-resolution diffraction techniques such as electron backscatter diffraction (EBSD) are excellent tools for studying the COR of hosts and oriented lamellae, as demonstrated by an increasing number of studies that have provided valuable insights into crystallization processes (e.g. Zhang et al. 2011; Proyer et al. 2013; Xu and Wu 2017). We significantly expand the available EBSD data for lamellae in garnet with analyses of 187 ilmenite, 96 rutile, and 31 apatite inclusions in garnet from metasedimentary gneiss ($T \geq 1000$ °C; P at least ~1.8 GPa) from the Brimfield Schist in the Central Maine Terrane of Connecticut, U.S.A. (Ague et al. 2013; Axler and Ague 2015b; Keller and Ague 2018). The inclusions are needle and plate shaped and the vast majority have SPO parallel to $<111>_{garnet}$. We combine these new data with those for 100 ilmenite, 250 rutile, and 180 corundum (Al_2O_3, trigonal) inclusions in garnet from eclogite facies metapegmatite in the Austrian Alps (Griffiths et al. 2016), metamorphosed at 600–750 ^oC and 1.8–2.4 GPa. These metapegmatites occur in a metamorphic sequence with eclogites, amphibolites, and metasedimentary rocks. Combining these datasets allows for comparison of samples with different geological histories to illuminate broad classes of garnet-oxide COR.

REVIEW OF ORIENTATION RELATIONSHIPS IN GARNET AND METALS

Orientation relationships in garnet

The number of published EBSD studies for COR of lamellar inclusions in garnet is fairly small, but growing. Recent work has used large (*n* > 200) datasets to examine the statistical prevalence of different COR between host garnet and lamellae of rutile, ilmenite, or corundum, both with and without SPO (Proyer et al. 2013; Griffiths et al. 2016). A number of different COR have been discovered for each of these garnet-oxide pairs, generating debate over formation mechanisms and the significance of COR for testing precipitation hypotheses (Hwang et al. 2007; Proyer et al. 2013; Hwang et al. 2016). Other studies, mostly with smaller datasets, have shown COR between host garnet and pyroxene (Spengler 2006; Zhang et al. 2011; Xu and Wu 2017), amphibole (Xu and Wu 2017), and rutile (Hwang et al. 2007; Xu and Wu 2017). Transmission electron microscopy (TEM) has also been used to examine the micro- and nano-scale relationships between garnet host and lamellae (Hwang et al. 2007; Proyer et al. 2013; Hwang et al. 2015, 2016).

Orientation relationships between garnet and lamellae may be classified as specific or statistical (Habler and Griffiths 2017). A specific COR is the exact alignment (within a few degrees) of multiple lamellae axes or planes to those of the host. Several sub-types of statistical COR exist, which describe alignment of lamellae axes either to host planes (a rotational feature), dispersed around host axes, or combinations of both. Some studies recognize as many as 24 different specific COR, subdivided by positive and negative Miller indices for equivalent directions (e.g. Hwang et al. 2016). Other studies, including ours, group COR into smaller numbers of specific or statistical groups.

Rutile is the most widely reported lamellae phase. A common rutile COR forms in different rock types. In their EBSD study of rutile lamellae in diamond-bearing metapelite garnet from the Greek Rhodope, Proyer et al. (2013) first reported that rutile lamellae with SPO//<111>$_{\text{garnet}}$ may have *c-axis* in a cone of 26–29° around <111>$_{\text{garnet}}$. Griffiths et al. (2016) later found the same COR in rutile both with and without SPO from metapegmatite garnets, but broadened the geometric criterion to a cone of 28.5° ± 2.5° around <111>$_{\text{garnet}}$ (Fig. 2). They also found that the relationship <103>$_{\text{rutile}}$//<111>$_{\text{garnet}}$ produces this COR (herein termed the "28.5° COR"). Rutile lamellae in UHP eclogites and gneisses may have the 28.5° COR as well (Hwang et al. 2015). Inclined extinction is a characteristic trait of rutile lamellae with the 28.5° COR because rutile *c-axis* and elongation direction are not parallel (Proyer et al. 2013; Griffiths et al. 2016). Inclined extinction has been reported in rutile lamellae from many different settings (Griffin et al. 1971; Hwang et al. 2007; Ague and Eckert 2012; Proyer et al. 2013; Hwang et al. 2015; Griffiths et al. 2016); some or all of these lamellae not yet characterized with EBSD may have the 28.5° COR.

Some preliminary EBSD data has been reported for apatite (Ruiz-Cruz and Sanz de Galdeano 2013), but large datasets suitable for in-depth crystallographic and statistical analysis were unavailable prior to the results we present below.

Lamellae formation hypotheses

The leading hypothesis for the formation of lamellae in garnet is solid-state precipitation (typically via exsolution) of phases containing trace elements soluble in the garnet structure at high-*T* and/or high-*P* conditions. In the classical exsolution interpretation, precipitates such as rutile, ilmenite, or apatite form via expulsion of impurities from the garnet structure as a result of retrogression. The energetics of this process, including a combination of thermodynamic favorability of nucleation over solubility in the garnet lattice, surface energy minimization, and strain energy minimization, among others, would control lamellae COR (Nabarro 1940; Fisher et al. 1952; Putnis 1992). Rigorous interrogation of lamellae origins is crucial if these textures are to be used as *P*-*T*, petrological, or geochemical indicators in geologic systems (e.g. Hacker et al. 1997; Wang et al. 1999; Hwang et al. 2007). Consequently, alternatives to lamellae precipitation from garnet must also be considered. The tenants, strengths, and weaknesses of several major hypotheses are laid out in Table 1, and detailed below.

One alternative hypothesis is emplacement of lamellar minerals along host cleavages or partings (e.g. Hwang et al. 2007, 2015). This hypothesis has not yet been supported by detailed explanation, experimental evidence, or theory to show how emplacement could produce such a regular 3-dimensional distribution of lamellae (Fig. 1b) in minerals like garnet which lack cleavage. This process would also be expected to leave clear textural evidence. Lamellae in the Connecticut (CT) samples are not found in uneven or isolated patches or along planar features, and commonly have SPO parallel to the host axes; these traits are also reported from other localities (e.g. Proyer et al. 2013; Hwang et al. 2015). This is strong evidence against an emplacement origin tied to cleavage planes (an additional serious complication being that garnet lacks good cleavage planes). Furthermore, any samples with concentric zones of precipitates, or crystal rims lacking precipitates, severely complicate this explanation (e.g. Proyer et al. 2013). Lamellae are also overwhelmingly limited to several microns in diameter (e.g. Hwang et al. 2007; Ague and Eckert 2012; Proyer et al. 2013; Axler and Ague 2015; Griffiths et al. 2016) except in rare cases from mantle settings (e.g. Griffin et al. 1971; van Roermund and Drury 1998). This size restriction is expected for a diffusion-controlled process such as precipitation but does not clearly follow for an emplacement origin. Although the emplacement hypothesis is important to consider in minerals with prominent cleavage such as pyroxene, it is inconsistent with the evenly-distributed lamellae observed in garnet (Fig. 1b-e).

Another non-precipitation hypothesis is simultaneous epitaxial co-growth of garnet and a lamellar phase or phases (Wang et al. 1999; Hwang et al. 2016). For example, epitaxial co-growth has been proposed to explain COR between dendritic titanomagnetite and clinopyroxene growing in melt (Hammer et al. 2010). In a case of diverse oriented oxide lamellae in kimberlitic pyrope, lamellae were interpreted as epitaxial crystallization products deposited on growing garnet crystal faces (Wang et al. 1999). Major limitations of this hypothesis for garnet, however, are that no oxide-garnet epitaxial relationships have been demonstrated, nor have garnet crystals been found with hair-like protrusions of oxides perpendicular to {111} or lying exactly along growth faces or edges. This hypothesis would also require garnet and lamellae to grow at essentially the same rate for extended periods, and no garnets with numerous rutile or other lamellae inclusions terminating exactly at the garnet crystal faces have been found. Moreover, despite many decades of experimental work involving growth of garnet from a wide variety of geologic fluid-mineral and melt-mineral systems, no oriented co-growth has been reported of which we are aware. Finally, oriented rutile lamellae are observed to cross-cut, and thus postdate, inclusion domains of matrix phases that garnet overgrew (e.g. Figs. 1c, d in Ague and Eckert, 2012). This clearly precludes hypotheses of rutile-garnet co-growth. Thus, co-growth remains unsubstantiated by natural or experimental evidence.

Both the emplacement and co-growth hypotheses require the growth of several simple oxide minerals from fluids or melts. The rocks with oxide lamellae in garnet that have been the subject of EBSD studies (Hwang et al. 2007; Proyer et al. 2013; Hwang et al. 2015; Hwang et al.

2016; Griffiths et al. 2016; Xu and Wu 2017) are from diverse settings and span a wide range of chemistries. It is highly improbable that they would have interacted with fluids and/or melts within the same narrow compositional range; moreover, no crustal or subduction zone fluids are known to precipitate simple oxides without a range of other minerals as well. These simple oxides that constitute lamellae suites, along with apatite in some cases, are formed of ions that have been shown to be soluble in garnet at high P and/or T (e.g. Ono 1998; Hermann and Spandler 2008; Ague and Eckert 2012; Konzett 2016; Ackerson et al. 2017a,b).

As noted above, many rutile lamellae in garnet also have inclined extinction, with crystallographic elongation oblique to the *c-axis* (Griffin et al. 1971; Hwang et al. 2007; Ague and Eckert 2012; Proyer et al. 2013; Griffiths et al. 2016). Critically, this characteristic has *never* been observed in free-standing idiomorphic rutile crystals in metamorphic or igneous rocks. Even in the well-known examples of epitaxial rutile nucleation on hematite, or “knee-twinned” (geniculated) hand samples, rutile is elongated parallel to the *c-axis* (e.g. Daneu et al. 2014; Rečnik et al. 2015). The lack of an explanation for this prominent crystallographic characteristic greatly weakens the emplacement and co-growth hypotheses, which posit the initial nucleation of a lamella either in a fluid phase or melt, or epitaxially on the garnet host. Inclined extinction is also found in rutile precipitates in star sapphire, where it is interpreted as evidence of rutile precipitation under the energetic constrains of the corundum lattice (Phillips et al. 1980; Boudeulle 1994). Analogous controls on solid-state rutile growth within a garnet lattice would explain why the lamellae have inclined extinction while free-standing euhedral rutile crystals do not.

Mineral replacement via interface-coupled dissolution-reprecipitation mediated by a fluid phase (ICDR; e.g. Putnis and John, 2010) can also involve co-precipitation. For example, monazite crystals produced during experimental ICDR of apatite can have an SPO with the apatite host (Harlov et al. 2005). Natural examples of monazite with SPO in apatite are also known (e.g. Amli 1975). Despite this, COR have not yet been reported from any laboratory ICDR experiments. In garnet, ICDR tends to produce distinct reaction fronts that propagate inward from host crystal margins or along cracks and that can be highly irregular (e.g. Pollok et al. 2008; Ague and Axler 2016; Keller and Ague 2018). This is clearly inconsistent with homogeneous or concentric distributions of lamellae. In the only published example of garnet with oriented lamellae *and* ICDR textures, lamellae are only present in the portion of the garnet core unmodified by ICDR (Keller and Ague 2018). This is strong evidence that lamellae were prevented from forming or were destroyed by ICDR. Regardless, the potential of ICDR to produce or modify COR in geologic materials is largely unexplored and further investigation is likely to be quite productive.

Equilibrium of minerals in garnet with respect to the rock matrix must be accounted for when considering non-precipitation hypotheses. For example, lamellae of corundum or aluminum hydroxides (e.g. Hwang et al. 2015) would not be in equilibrium with a fluid present in a quartz-saturated rock. Unless wholesale bulk rock chemistry changes took place, emplacement hypotheses for aluminum oxide lamellae within garnet in quartz-saturated rocks are difficult to envision. Such lamellae may in fact be the product of unmixing reactions operating at nano- to micrometer-scale local equilibrium, shielded by the garnet host from the influence of rock matrix chemistry.

Some of these lamellae growth hypotheses, particularly emplacement, can appeal to fluid-mediated processes. As such, the small pockets of fluid, hydrous phases, and amorphous layers at host-lamellae contacts observed in some settings have been suggested as evidence of lamellae growth from a fluid (e.g. Hwang et al. 2007, 2015). While the presence of these structures is a valuable observation, this explanation is complicated by the solubility of H^+ in the structures of some minerals such as rutile at reducing or high-*T* conditions (e.g. Colasanti et al. 2011). If a rutile formed as a precipitate at such conditions, the formerly soluble H^+ would naturally be expelled during retrogression due to the experimentally documented high diffusivity of H^+ in rutile (Colasanti et al. 2011). This could create a small amount of fluid, hydrous mineral, or amorphous substance at the rutile-garnet contact. Other constituents soluble in rutile at elevated *P*-*T* conditions, such as Al (Zack et al. 2004; Escudero et al. 2012; supplementary data of Ague et al. 2013), could also be expelled contributing to such processes by forming, for example, Al hydroxides. In addition, garnet can hold up to several thousand ppm water in its structure (e.g. Ono 1998; Song et al. 2005; Konzett 2016 and references therein). This could be imparted to umixing precipitates or expelled around them. Finally, precipitates may nucleate on inclusions of fluid (or melt) in the host; the fluid becomes incorporated along host-precipitate contacts as the precipitate grows (Axler and Ague 2015b). In summary, the presence of micro-pockets of fluid, hydrous phases, or amorphous material at host-lamellae interfaces is not definitive evidence of lamellae crystallization directly from fluid or melt, particularly if systematic COR are present. We note, however, that exsolution may be enhanced in the presence of fluid (Zhao et al. 2017).

An additional proposed lamellae-forming hypothesis is open system precipitation (OSP) (Proyer et al. 2009; Proyer et al. 2013). This involves exchange of ions with the matrix or internal inclusions, whether through oxidation-reduction reactions, diffusion, or some other transport process. As a result, host diffusion rates, kinetics, and solid solution will be important mineralogical controls on OSP. Open system precipitation does not entail emplacement, entrapment, or co-growth of lamellae, but rather precipitate growth from key components (e.g. TiO_2 for rutile) originally contained within the host as in classical closed-system exsolution. Consequently, lamellae precipitated via OSP would be expected to have the same possible COR as those produced by traditional closed-system precipitation. It is critical to note that there is no documentation that Ti or phosphorus would diffuse *into* garnet during retrogression to produce lamellae (e.g. Proyer et al. 2013; Axler and Ague, 2015a).

Operation of OSP allows for the precipitation of minerals like rutile, which cannot unmix stoichiometrically from garnet. One documented OSP example is the loss of Na from UHP garnet when rutile and apatite precipitates form (Axler and Ague, 2015a). Other OSP formulations postulate that dodecahedral Fe^{2+} is oxidized to octahedral Fe^{3+} and/or that divalent cations coupling Ti^{4+} substitution in garnet are lost instead of forming precipitates (Proyer et al. 2013).

Open-system precipitation is not required to explain precipitation of minerals soluble in garnet as solid solution endmembers, such as pyroxene (in majoritic garnet). In addition, laboratory experiments have produced synthetic near-endmember almandine garnet with significant crystallographic defects that allow for accommodation of impurities such as OH^- and Fe^{3+}; reactions decomposing such defects have been proposed to produce oxide lamellae including rutile (Geiger et al. 2016). Such a scenario would not require open-system precipitation.

The term “exsolution” has historically been used in the geological literature to denote solid-state precipitation, assuming closed-system behavior. Given the relevance of OSP to precipitation of rutile from garnet we use the term precipitation in a general sense to denote the family of unmixing processes including exsolution and OSP, as well as other possibilities such as grain boundary migration which may induce precipitation (e.g. Cahn et al. 1979; Baumann et al. 1981), and spinodal decomposition (e.g. Cahn and Hilliard 1971; Sánchez-Muñoz et al. 2016). Any of these processes require the essential lamellae nutrients to have been held within the garnet solid solution, and therefore all have the same petrologic and tectonic implications for the host garnet.

Finally, a host of other mechanisms have been postulated to explain lamellae in garnet, including recrystallization of non-lamellar oxide inclusions at high temperature, overgrowth of oriented matrix oxides, etching of host garnet surfaces by fluid action followed by oxide deposition into the channels, or reactions with melt. These have been dismissed because they have not been observed in geologic systems, have not been shown to apply to garnet-oxide systems specifically, or simply appeal to extraordinary coincidence (some examples are given in Table 1; see detailed discussion in Proyer et al. 2013). Nonetheless, alternative hypotheses are important to consider so that precipitation can be tested rigorously. We build on previous work by examining garnet-lamellae COR in the context of the many studies devoted to COR in metals, both natural and anthropogenic.

Orientation relationships in metals

Alloys have received widespread microstructural study due to their societal usefulness. Many alloys develop the Widmanstätten pattern, a precipitation structure in which close-packed planes are aligned: $\{110\}_{\text{lamella}}//\{111\}_{\text{host}}$ (e.g. Goldstein and Ogilvie 1965; Bunge et al. 2003; Stanford and Bate 2005; Sonderegger et al. 2007; Cayron 2014) (Fig. 1a). Widmanstätten-type patterns form during the γ–α taenite–kamacite transformation in meteoritic nickel-iron

(Goldstein and Ogilvie 1965; Bunge et al. 2003; Cayron 2014), martensitic transformations in steels (Sonderegger et al. 2007), and the β-α transformation in brass (Stanford and Bate 2005), the latter two studied under extremely well-constrained, closed-system laboratory conditions. Two common COR are recognized: the Nishiyama-Wasserman ($<110>_{lamella}//<112>_{host}$) and Kurdjumov-Sachs (or Young-Kurdjumov-Sachs) ($<111>_{lamella}//<110>_{host}$) (NW and KS, respectively) (Bunge et al. 2003; Sonderegger et al. 2007; Cayron 2014), which are connected by a 60° rotational relationship to $<111>_{host}$ (Bunge et al. 2003; Morito et al. 2006). Diffraction studies using high-resolution modern methods show that there is continuity between the NW and KS COR (Bunge et al. 2003; Sonderegger et al. 2007; Cayron 2014). Metals represent ideal cases for studying COR because they can be created on short timescales in laboratory experiments and compared to natural samples from meteoric alloys. Lamellae with COR in alloys are the gold standard for precipitation structures formed free of the open-system emplacement processes cited as a complicating factor in geological systems with prolonged metamorphic histories and crystal annealing. We will return to the Widmanstätten pattern in our discussion of rutile COR below.

MATERIALS AND METHODS

Samples, Petrography, and Imaging

Rock samples of metapelitic gneiss were collected from the study area in northern Connecticut, USA (N41.873164°, W72.275133°). Petrographic thin and thick sections were prepared and polished at Yale University using successive SiC grit, diamond paste, and 0.05 μm colloidal silica suspension. Lamellae were selected for analysis if they had elongated (needle-like or plate-like) forms and a clear <111>$_{garnet}$ SPO, or if lacking defined forms, were part of a composite lamella with a clear <111>$_{garnet}$ SPO. Irregularly-shaped and other non-lamellar inclusions that could be, for example, matrix phases overgrown by garnet are not included in the data set. These comprise <10% of the investigated inclusion population. Each lamella was characterized mineralogically and texturally in thin section using a transmitted light/reflected light Leitz SM-LUX-POL petrographic microscope. Lamellae were photographed and their locations indexed for EBSD analysis. The vertically-integrated thin section images of Figures 1b-e were captured using a Leica DMC2900 camera attachment and LASv.4.10 software. A single image was built while the microscope was manually focused through the depth of the thin section.

Scanning Electron Microscopy and Electron Backscatter Diffraction

Thin sections were warmed in a 50°C oven overnight to remove surface moisture. A carbon coat of 8–11 nm was applied in a vacuum chamber immediately before loading into the electron microscope to boost sample surface conductivity. Small amounts of colloidal silver solution were placed at the contacts between conductive tape and the sample surface to reduce surface charging. EBSD measurements were made with the FEI 30x ESEM at Yale University. EBSD spot analyses used a working distance of 20 mm, a sample tilt of 70°, accelerating voltage of 15kV, beam current of ~2 nA, and a beam spot size of 5 (allowing for analysis of ~1–2 μm diameter lamellae) with minimum vacuum strength of $1e^{-4}$ Pa. Data were collected using Oxford Instruments HKL Channel 5 Flamenco software. Before making spot analyses, backgrounds were acquired in the polygranular rock matrix using a minimum time per frame of 150 to 200 ms and 2x2 binning. Each sample background was used for all analyses in the sample. Multiple spot analyses of host garnet were collected for each grain to ensure that garnet hosts were single crystals. Band detection limits were set to 5 (min) and 6 (max). Only spot analyses with mean angular deviation (MAD) ≤1° were accepted. All data for each garnet were collected in a single analysis session.

Data Analysis and Plotting

All datasets were rotated to the same frame of reference parallel to <100>$_{\text{garnet}}$ to allow for comparative analysis. Data analysis and pole figure plotting used the MTEX toolbox (Bachmann et al. 2010; Hielscher et al. 2010) in MATLAB. Copies of each dataset were rotated around the 4-fold axis used as the frame of reference to produce a "symmetrized" plot, following the method of Griffiths et al. (2016). All pole figures are equal angle, antipodal, upper hemisphere stereographic projections. Orientation distribution function plots (Figs. 3a, 4a, 5a, 7a) were made using the MTEX toolbox 'calcODF' function and a kernel halfwidth of 7°, and were plotted as equal angle projections. The ODF calculations use single copies of each data set, not the symmetrized versions.

The same COR selection criteria used for the CT samples were also applied to the data provided in the supplementary materials of Griffiths et al. (2016). The major difference between the datasets is that the Griffiths et al. (2016) lamellae have a less well developed SPO. They describe the analyzed inclusions as "equant or slightly oblate, with no shape-preferred orientation," although they do note two exceptions: corundum is found as tabular crystals with a pronounced elongation direction and some rutile crystals have acicular habits with the long axis parallel to <111>$_{\text{garnet}}$. This SPO is dominant for rutile as well as ilmenite and apatite in the CT samples (Fig. 1b-e).

We compared two slightly different COR search criteria: the COR groupings of Griffiths et al. (2016) and a new scheme developed herein grounded in the Griffiths (2016) groupings (Fig. 2). The major difference between the two systems is that we do not use the 5°–22° cone around <110>$_{\mathrm{garnet}}$ as a rutile COR because it has extensive angular overlap with *c-axis* in {111}$_{\mathrm{garnet}}$, and also with the 28.5° COR (Fig. 2). Griffiths et al. do not consider *c-axis* in {111}$_{\mathrm{garnet}}$ as a rutile COR, and do not consider the 5°–22° cone COR for other minerals. Both of these COR are statistical, but the {111}$_{\mathrm{garnet}}$ COR is present for multiple lamellae minerals (Tables 2 and 3), indicating some broad control over inter-mineral lamellae COR. We have also identified no low-Miller index garnet axes unique to the 5°–22° cone COR to which lamellae fit. We therefore suggest that lamellae with *c-axis* aligned to a low-Miller index garnet feature, such as *c-axis* in {111}$_{\mathrm{garnet}}$, be sorted into that COR, with the remainder interpreted as having no COR. In rare cases where a lamella satisfied two different COR, we grouped it with the more prevalent COR. Removing the 5°–22° cone COR also makes statistical COR criteria more consistent and more selective by only allowing minor angular deviations (5°) from primary garnet crystallographic structures (Fig. 2). Our COR methodology considers the same set of COR between all analyzed minerals, which simplifies the COR selection process, and results in a lower proportion of lamellae with COR from each locality relative to the Griffiths et al. (2016) COR criteria (Tables 2 and 3). Complete EBSD data for apatite, ilmenite, and rutile analyzed in this work are provided in Supplemental Table S1. Data of Griffiths et al. (2016) are available in the supplemental materials of their work.

The *d*-spacing ratios of host-lamellae pairs were calculated by selecting appropriate unit cell parameters from the range of mineral compositions relevant to the rock's bulk composition (Table 4). Calculations used room temperature and pressure values after the method of Griffiths et al. (2016), who found negligible difference in lattice strains calculated using room temperature values and ~600 °C values.

RESULTS

EBSD Data

We compared EBSD results for rutile and ilmenite between the CT and Austria localities and, together with corundum from the Austrian locality and apatite from the CT locality, consider all of these minerals to study COR trends. Because many lamellae have *c-axis* parallel to the $\{111\}_{\text{garnet}}$ plane, in this work we use the phrase "within $\{111\}_{\text{garnet}}$" to mean that a vector is parallel to the {111} plane. Several garnet axes, including $<110>_{\text{garnet}}$ and $<112>_{\text{garnet}}$ are within $\{111\}_{\text{garnet}}$; consequently we grouped all lamellae axis fits to any structure within the $\{111\}_{\text{garnet}}$ plane (Tables 2 and 3). This simplifies COR classification by grouping structures that are angularly equivalent (i.e. all points on $(111)_{\text{garnet}}$ are 90° from $[111]_{\text{garnet}}$) and facilitates comparison of overarching trends between localities. Several specific COR are recognized within the broader category of lamellae with *c-axis* in $\{111\}_{\text{garnet}}$. These are reported for both the CT and Austria datasets in Supplemental Table S2.

Both localities have similar garnet-oxide COR (Tables 2 and 3). We find that ilmenite from the CT locality has the same COR as ilmenite from the Austrian locality, and for the most part in comparable proportions (Table 2). Ilmenite and corundum also share many COR, as found by Griffiths et al. (2016). Ilmenite from both localities and corundum preferentially align $<11\bar{2}0>$ or less commonly $<10\bar{1}0>$ with $<111>_{\text{garnet}}$, which necessitates that the perpendicular *c-axis* falls within $\{111\}_{\text{garnet}}$ (Figs. 3c, 4b). Ilmenite from both localities and corundum may also have *c-axis*//<111>$_{\text{garnet}}$, but this is more prevalent for corundum than ilmenite, and both minerals mostly avoid aligning *c-axis*//<100>$_{\text{garnet}}$ (<1% from CT and 2% or less from Austria; Table 2).

The most prevalent rutile COR for both localities is to have *c-axis* within a ~28.5° cone around <111>$_{\text{garnet}}$ caused by the statistical COR <103>$_{\text{rutile}}$//<111>$_{\text{garnet}}$ (Fig. 5; Table 3). The size of this cone varies slightly by report: the value given by Griffiths et al. (2016) is 28.5° ± 2.5°, while Proyer et al. (2013) report an average angle of 27.6°. We group all rutile satisfying the angular criteria of either Proyer et al. (2013) or Griffiths et al. (2016) into the "28.5° COR." Rutile *c-axes* are distributed unevenly around the circumference of the cone and concentrate around <135>$_{\text{garnet}}$ and <134>$_{\text{garnet}}$ (Hwang et al. 2016). Rutile with the 28.5° COR are elongated obliquely to the *c-axis* and therefore have inclined extinction.

Both localities also show several other rutile COR. The second most common COR is *c-axis*$_{\text{rutile}}$//<110>$_{\text{garnet}}$. Rutile may also have *c-axis* within {111}$_{\text{garnet}}$, or rarely *c-axis*$_{\text{rutile}}$//<111>$_{\text{garnet}}$ or *c-axis*$_{\text{rutile}}$//<100>$_{\text{garnet}}$ (Table 3, Fig. 5a). Slightly less than 30% of rutile do not fit into any of the above categories. Because we did not use the "*c-axis* between 5° and 22° from <110>$_{\text{garnet}}$" COR of Griffiths et al. (2016), we sorted these rutile lamellae into the "*c-axis* in {111}$_{\text{garnet}}$" COR category, or as having no COR (Table 3).

In addition, we recognize a rutile-specific COR that has a relationship with host garnet analogous to that between host taenite and lamellar kamacite in a Widmanstätten pattern (the "Widmanstätten-type COR"). This group has the 28.5° COR but also has *c-axis* in {111}$_{\text{garnet}}$ and aligns <110> within ~2° of <111>$_{\text{garnet}}$; it is noted as COR-2 by Hwang et al. (2015, 2016) as an occurrence maximum within the 28.5° COR. The extraordinary distinguishing characteristic we report here is that stereographic projections of poles to {302}$_{\text{rutile}}$ that have <110>$_{\text{rutile}}$//<111>$_{\text{garnet}}$

are almost identical to those of kamacite lamellae with the NW and KS ORs in iron meteorites (Fig. 6a-d) (Bunge et al. 2003). These kamacite lamellae align one of the six $<110>_{\text{kamacite}}//<111>_{\text{taenite}}$ and trace 60° cones about $<111>_{\text{taenite}}$ with the other five $<110>_{\text{kamacite}}$. In the tetragonal rutile lattice, the pole to {302} which exhibits the same type of behavior is at a 44° angle to $[001]_{\text{rutile}}$, making it angularly very similar to $<101>_{\text{isometric}}$ (the poles to dodecahedral faces, at 45° to $<001>_{\text{isometric}}$).

Based on this remarkable similarity, we define the Widmanstätten-type specific COR according to: (1) $<103>_{\text{rutile}}//<111>_{\text{garnet}}$; (2) *c-axis* within $\{111\}_{\text{garnet}}$; (3) $<110>_{\text{rutile}}//<111>_{\text{garnet}}$; and (4) poles to $\{302\}_{\text{rutile}}$ that lie on 60° cones around $<111>_{\text{host}}$ (Fig. 6e-f). The first three traits were recognized by Hwang et al. (2015, 2016) but the fourth is crucial to the COR interpretation. The Widmanstätten-type COR makes up nearly 40% of the 28.5° COR for the CT samples, and roughly 20% for the Austrian ones. As the 28.5° COR is a statistical COR covering all of the rotational space within the 28.5° ± 2.5° cone, there is clearly some preference for this specific orientation within the 28.5° COR.

Both localities show a greater variety of rutile COR than are reported from acicular rutile lamellae in diamond-bearing garnet from the Greek Rhodope (Proyer et al. 2013) but this may be an artifact of progressive development of COR selection criteria in recent years. The Greek locality appears to have a higher proportion of rutile lamellae with the 28.5° COR than either the CT or Austria locality (Fig. 2a of Proyer et al. 2013).

We also present the first extensive dataset for apatite COR in garnet. Apatite preferentially aligns *c-axis*$//<111>_{\text{garnet}}$ (Table 2; Fig. 7a). Of the apatites with this COR, 68% also align $<11\bar{2}0>_{\text{apatite}}//<112>_{\text{garnet}}$ and $<10\bar{1}0>_{\text{apatite}}//<110>_{\text{garnet}}$, meaning 48% of all analyzed apatites have the same specific COR. This dominance of a single specific orientation is different from the observed behavior of rutile, ilmenite, and corundum, which primarily have statistical COR such as the 28.5° COR for rutile, or *c-axis* within $\{111\}_{\text{garnet}}$ for the trigonal oxides. Nonetheless, corundum and ilmenite lamellae from both localities can have the specific COR of apatite (Table 2).

The COR *c-axis*$_{\text{apatite}}$//<111>$_{\text{garnet}}$ was noted in garnet from the UHP Rif Complex (Ruiz-Cruz and Sanz de Galdeano 2013), but the authors do not specify what proportion of apatite has this COR. They also report apatite *c-axis*$_{\text{apatite}}$//<100>$_{\text{garnet}}$, which is not observed in our samples, and *c-axis*$_{\text{apatite}}$//<110>$_{\text{garnet}}$, which we find for a single lamella. Considering the presence of the *c-axis*$_{\text{apatite}}$//<111>$_{\text{garnet}}$ COR across rock types and metamorphic conditions, and given its clear dominance in the CT samples, *c-axis*$_{\text{apatite}}$//<111>$_{\text{garnet}}$ is likely a preferred COR for apatite.

ODF Calculations

Orientation distribution function (ODF) plots for each lamellae species in garnet demonstrate that coincidence of lamellae axes with garnet structure is highly statistically significant (Figs. 3a, 4a, 5a, 7a). The rutile ODF plots for the two localities appear different because the Austrian samples have ~10% more rutile with *c-axis*//<110>$_{\text{garnet}}$ while the CT samples have ~10% more rutile with the 28.5° COR. Otherwise, COR distributions between the localities are quite similar, and both localities have nearly identical total amounts of rutile with COR (Table 3). Differences of axial distribution within a statistical COR may prove useful as a petrogenetic indicator if they can be tied to differences in, for example, *P*-*T* path or tectonic setting. The greatest difference between the localities for a lamella species is that ilmenite in the Austrian samples commonly has *c-axis*//<111>$_{\text{garnet}}$ (20%, Table 2), whereas this COR is much less common (5%) in the CT samples. The comparable ODFs of ilmenite and corundum mirror their nearly identical distributions of COR (Figs. 3a, 4a). The intense loci of the apatite ODF reflect the dominance of the *c-axis*$_{\text{apatite}}$//<111>$_{\text{garnet}}$ COR (Fig. 7a).

COR PREDICTION

Multiple studies of lamellae COR in garnet have attempted to predict which COR will form based on host and lamellae crystallography. One method evaluates the lattice strain at the host/lamellae interface following the coherent lattice matching model (e.g. Howe 1997; Balluffi et al. 2005). Griffiths et al. (2016) calculated strain using the percentage difference between garnet and lamellae *d*-spacings, setting a 4% threshold for a good fit. They concluded that the method cannot predict the favorability of observed CORs. Hwang et al. (2016) used a combination of lattice point matching (coincident site lattice; e.g. Brandon 1966; Santoro and Mighell 1973; Fujii et al. 2018) and polyhedron matching to evaluate the unconstrained lattice mismatch between garnet and rutile lamellae and concluded that most rutile COR did not have favorable matches.

We assessed strain by calculating the *d*-spacing ratios of garnet and lamellae planes with low Miller indices (i.e. those that intersect atoms in the lattice and form crystal faces), without setting a fixed threshold for selecting best fit. According to the lattice matching model, the lowest strain arises with *d-spacing* ratios close to 1:1 (e.g. Howe 1997). We find that such calculations can successfully predict several specific COR.

For example, apatite has a single dominant specific COR ([0001]$_{\text{apatite}}$//<111>$_{\text{garnet}}$ with <$10\bar{1}0$>$_{\text{apatite}}$//<110>$_{\text{garnet}}$ and <$11\bar{2}0$>$_{\text{apatite}}$//<112>$_{\text{garnet}}$; Table 2). This has low-strain planar matches in three directions, all with *d*-spacing ratios near 1:1, namely: (0001)$_{\text{apatite}}$//{111}$_{\text{garnet}}$,

$\{10\bar{1}0\}_{apatite}$//$\{110\}_{garnet}$, and $\{11\bar{2}0\}_{apatite}$//$\{112\}_{garnet}$ (Table 4). Low strain for three non-parallel planar matches explains why apatite commonly has a single specific COR rather than a statistical COR. Indeed, the calculations successfully predict the major observed COR. These are the first strain calculations for apatite lamellae in garnet of which we are aware.

Moreover, apatite's strong preference to align *c-axis*//$<111>_{garnet}$ may mean that the oxygen chains along $<111>_{garnet}$ can influence lamellae COR formation. The *c-axis* in apatite is the close-packed oxygen direction, and >70% of apatite lamellae have their close-packed oxygen direction parallel to that of the host garnet. This is evidence that in some cases lamellae crystallographic orientation could be related to minimization of oxygen diffusion length, with close-packed oxygen direction of host ($<111>_{garnet}$; Andersson and O'Keeffe 1977) becoming that of precipitate. This trait has been noted for rutile precipitates in star sapphire (Phillips et al. 1980; Boudeulle 1994), and analogously for precipitation in metallic systems, where close-packed rows of metal atoms align in the KS COR (e.g. Shiflet and van der Merwe 1994; Bunge et al. 2003; Sonderegger et al. 2007).

Ilmenite and corundum also have the specific COR common in apatite: [0001]//$<111>_{garnet}$ with $<10\bar{1}0>$//$<110>_{garnet}$ and $<11\bar{2}0>$//$<112>_{garnet}$ (Table 2), although it is not the dominant COR observed in these phases. This specific COR has the same planar matches for both minerals as it does in apatite; however, the *d*-spacing ratios are about 1:2 or 2:1, not 1:1 as for apatite (Table 4). These ratios may account for the fact that this COR is not as abundant for ilmenite and corundum as it is for apatite. Nonetheless, its existence across three lamellae pairs supports the predictive capability of strain calculations for certain specific COR. Interestingly, the Austrian samples show a higher proportion of ilmenite with this COR than the CT samples (Table 2).

For the classic precipitation texture of Widmanstätten patterns in meteoric nickel-iron, strain calculations predict the existence of the specific NW and KS CORs, which both have the lowest-strain alignment $\{110\}_{\text{kamacite}}//\{111\}_{\text{taenite}}$ with a near 1:1 *d*-spacing ratio (Table 4). Although this represents only one key planar *d*-spacing match, these planes are the closest-packed in their structures which is likely favorable for precipitation (e.g. Hutchinson et al. 2005; Tan et al. 2016).

Remarkably, as demonstrated above, the Widmanstätten-type COR is predicted in rutile by the same match as in metals: $\{110\}_{\text{rutile}}//\{111\}_{\text{garnet}}$ (Table 4). The Widmanstätten-type COR is a specific COR that has $<110>_{\text{rutile}}$ within 5° of $<111>_{\text{garnet}}$, as well as $<103>_{\text{rutile}}//<111>_{\text{garnet}}$ and $c\text{-}axis_{\text{rutile}}//\{111\}_{\text{garnet}}$. Hwang et al. (2016) showed that this group (their COR-2) has the calculated lowest-strain lattice match and optimal polyhedral alignment with garnet $<103>_{\text{rutile}}//<111>_{\text{garnet}}$ and $<010>_{\text{rutile}}//<4\bar{3}\bar{1}>_{\text{garnet}}$. They interpreted this as compelling evidence of precipitation. We also consider the COR to be indicative of precipitation because Widmanstätten patterns are unquestionably a precipitation texture produced as a result of cooling (e.g. Ramsden and Cameron 1966; Bunge et al. 2003; Cayron 2014). A tetragonal phase has even been identified in Widmanstätten patterns, which may indicate initial nucleation of a tetragonal precipitate in the isometric host taenite (Ramsden and Cameron 1966). This might explain why rutile is capable of forming an equivalent relationship with its isometric host.

These results show that strain calculations, in concert with other crystallographic evidence, may predict dominant specific COR as exemplified by apatite and alloys. The *d*-spacing ratios that predict specific COR for rutile, ilmenite, and corundum are all 1:2 or 2:1 and therefore represent higher strain, but appear to be at least local energetic minima. The predicted specific COR is less common in these minerals than in apatite, for which it likely represents a global energetic minimum given both the near 1:1 ratios for three non-parallel *d*-spacing relationships as well as the parallelism of close-packed directions for apatite and garnet along $<111>_{\mathrm{garnet}}$.

Importantly, statistical COR are for the most part not predicted, nor are all specific COR predicted, such as those in Supplemental Table S2. Furthermore, some low-strain (near 1:1 or 1:2) matches in Table 4 are unrepresented by common COR. We suggest that these may be less favored as they have only one *d*-spacing match, unlike apatite, ilmenite, and corundum which have three. Nonetheless, it is also true that the Widmanstätten-type COR has only one key planar match in alloys and rutile for the low-index planes investigated. However, in these cases, other crystallographic factors may play an additional important role, including matching of closest-packed planes in alloys and the optimal polyhedral alignment for rutile.

Other emerging methods may help predict COR. While there is no low-strain planar match that predicts the statistical 28.5° COR in rutile (the relationship $<103>_{\mathrm{rutile}}//<111>_{\mathrm{garnet}}$), Griffiths et al. (2016) noted that $<103>_{\mathrm{rutile}}$ has a 1:2 vector length ratio with $<111>_{\mathrm{garnet}}$, meaning the lattice dimensions are rational multiples along those vectors. As the 28.5° COR is preferred for rutile across multiple localities (Proyer et al. 2013; Hwang et al. 2016; Griffiths et al. 2016; Xu and Wu 2017), this vector length relationship is well worth further investigation. The approach comparing parallel host and lamellae symmetries for different COR also holds promise (Griffiths et al. 2016). The prevalence of the apatite specific COR across three minerals with 3- or 6-fold symmetry parallel to the *c-axis* is the best evidence yet that COR may be influenced by symmetry. Garnet has 3-fold symmetry along <111>, to which the trigonal and hexagonal lamellae minerals align their 3-fold or 6-fold axis for the predicted specific COR (Table 4).

Another example is the tendency of rutile have its *c-axis* at an angle to <111>$_{\text{garnet}}$, which may reflect the symmetry mismatch between the 4-fold rutile axis and the 3-fold garnet axis.

A further notable result is that regardless of whether the COR is statistical or specific, ilmenite, corundum, and apatite consistently align one primary crystallographic axis within 5° of that of <111>$_{\text{garnet}}$. This places: (1) a lamellae axis parallel to the close-packed direction <111> in garnet along which octahedral sites are linked and (2) low-index planes of lamellae parallel to {111}$_{\text{garnet}}$ (Figs. 3, 4, and 7). Parallelism of low-index planes at the host-lamellae interface is considered indicative of a low-energy interfacial configuration (e.g. Rohrer 2011; Marquardt et al. 2015).

DISCUSSION

We evaluate the precipitation hypothesis considering the crystallographic data and textural observations from varying rock types and occurrences.

The percentage of lamellae minerals with identified COR is high: 80–96% using the Griffiths et al. (2016) classification, and 72–94% using our somewhat more conservative approach (Tables 2 and 3). Interestingly, all lamellae show a range of COR, particularly rutile, ilmenite, and corundum. The presence of multiple COR strongly suggests that the thermodynamic driving force to expel minor or trace constituents from the garnet lattice is very powerful during cooling and/or exhumation leading to precipitation even if ideal matching with the garnet lattice is not possible or achieved. Indeed, garnet and lamellae have very different structures which means that there will always be some misalignment between host and precipitate lattices, resulting in crystallographic degrees of freedom facilitating multiple COR.

Nucleation could occur on diverse micro- or nanostructural features including edge dislocations, screw dislocations, vacancies, interstitials, fluid inclusions, and even other lamellae nuclei (e.g. Cahn 1957; Putnis 1992; Axler and Ague 2015a). Each of these nucleation styles, as well as simple homogeneous nucleation, could cause formation of different sets of COR. Notably, multiple COR are reported in many alloys (e.g. Stanford and Bate 2005; Morito et al. 2006; Cayron 2014), so the presence of multiple COR for lamellae in garnet clearly does not disqualify the precipitation hypothesis, as has been suggested (Hwang et al. 2016).

Lattice parameters for minerals such as garnet with extensive solid solution may change during metamorphism as composition evolves at different *P*-*T* conditions. If a garnet preserved greatly different compositions in cores compared to rims, this might be reflected in COR if lattice parameters exert strong controls on COR formation. Spatial variation of COR has been suggested, but remains relatively unexplored (Griffiths et al. 2017). Many crystallographic factors in addition to composition could potentially influence such variations. For example, if one region of a garnet had a high density of dislocations upon which lamellae nucleated (e.g. surrounding ruptured inclusions, Axler and Ague 2015a), more lamellae in that region might have COR, or proportions of COR varieties, that differ from those in other parts of the crystal. This could lead to the development of different SPO patterns, as could preferred growth of lamellae parallel or subparallel to the directions of diffusion of lamellae-forming constituents such as Ti through garnet.

The CT and Austrian localities have markedly different geological histories, yet rutile and ilmenite lamellae have the same COR varieties, as well as mostly similar, although not identical, distributions of COR (Tables 2 and 3). Consequently, it is highly implausible that these first-order traits are a result of, for example, emplacement, co-growth of lamellae and garnet, or matrix growth of lamellae that were subsequently overgrown by garnet (Table 1). If such were the case, controlling factors such as garnet growth rate, fluid chemistry, dislocation density, strain rate, annealing rate, exhumation rate, and retrograde deformation that naturally differ between localities would be expected to produce strongly non-overlapping sets of COR.

It is likewise difficult to sustain the idea that some lamellae precipitated while others were emplaced or formed by some other mechanism simply because some lamellae lack identifiable COR (Hwang et al. 2016). In the CT samples (we have not examined the Austrian samples), lamellae with COR are commonly found adjacent to, or even intergrown with, other lamellae without COR. These lamellae are spatially associated on the micron scale and are visually indistinguishable. In addition, some lamellae that apparently lack COR may actually have COR that remain to be identified. It is also worth noting in this context that nucleation on dislocations may produce precipitates that lack COR altogether (Cahn, 1957).

Observed COR properties vary widely between lamellae minerals, but the shared characteristic of the vast majority of the CT lamellae is SPO parallel to the close-packed $<111>_{garnet}$ direction (Fig. 1b-e). Furthermore, nearly all rutile and a large fraction of ilmenite lamellae with COR described herein are elongated oblique or at 90° to their *c-axis* (where SPO is present). As far as we are aware, euhedral crystals of these same minerals never manifest such habits, which should be considered strong evidence of growth conditions different than “normal” examples in rock matrices. Oblique elongation produces inclined extinction in rutile (Griffin et al. 1971), another trait not observed in free-standing well-crystallized examples. Although the CT samples have strong SPO, it is also true that SPO is clearly not a prerequisite for COR, as many lamellae in the Austrian samples lack SPO (Griffiths et al. 2016).

Methods for predicting COR are still in their infancy, but simple quantitative and qualitative approaches can be successful in some cases. Two examples stand out. First, we show that the dominant COR observed for apatite is specific and has low-strain planar matches in three directions, all with *d*-spacing ratios near 1:1 relative to host garnet: $(0001)_{\text{apatite}}//\{111\}_{\text{garnet}}$, $\{10\bar{1}0\}_{\text{apatite}}//\{110\}_{\text{garnet}}$, and $\{11\bar{2}0\}_{\text{apatite}}//\{112\}_{\text{garnet}}$ (Table 4). Furthermore, apatite lamellae align their close-packed direction $[0001]_{\text{apatite}}$ parallel to that of garnet $<111>_{\text{garnet}}$. This is the first instance of which we are aware of that simple strain and close-packing arguments have been successful in predicting the dominant COR for a lamellae phase in garnet. Furthermore, we observe this same COR in ilmenite and corundum. It is not as common for these phases, probably because the lattice matching is about 1:2 or 2:1 with host garnet, not 1:1 as in apatite. Regardless, the specific COR common to apatite is also shared by ilmenite, and corundum, which do not share chemistry, oxygen sublattices, or *d*-spacings.

Second, the presence of the Widmanstätten-type COR for rutile in garnet is a striking parallel with alloys. This specific COR, defined by $\{110\}_{\text{rutile}}//\{111\}_{\text{garnet}}$ (Table 4), may characterize as much as 20% of the rutile lamellae from a locality (Table 3). Furthermore, our analysis of the large (*n*=213) dataset of Proyer et al. (2013) shows that it is present for rutile in diamond-bearing garnet from the Greek Rhodope. Moreover, Hwang et al. (2015) found it for rutile needles in star garnet from Idaho, as well as in garnet from the Sulu UHP terrane and diamond-bearing rocks from the Erzgebirge. It is also present for 36% of rutile lamellae in garnet from the UHP Lüliangshan garnet peridotite in China (Xu and Wu 2017). Widmanstätten patterns are unequivocal exsolution structures formed by gradual cooling. The ability of rutile to align lattice planes with garnet to form the equivalent of an isometric/isometric COR angularly transposed into an isometric/tetragonal system clearly indicates a preference for the lowest-energy host-lamellae configuration, and is fully consistent with the crystallographic analysis of Hwang et al. (2016).

Precipitation from a garnet host as envisioned herein requires that the lamellae form from chemical constituents pre-existing in the garnet lattice. For example, the presence of nutrient depletion halos around lamellae in the CT samples and also the UHP garnets of the Erzgebirge (Ague and Eckert 2012; Axler and Ague 2015a) demonstrates that lamellae drew components from garnet during their growth. If precipitation is by exsolution, then diffusion is the mode of transport. The operation of diffusion raises the possibility of material leaving as well as entering the crystal. This is postulated for the OSP model of Proyer et al. (2013). Indeed, garnet rims diffusively lost Ti at the CT locality during retrogression and the rims lack lamellae (Ague and Eckert, 2012). Presumably the Ti was imparted to the rock matrix, depleting the rims so that no Ti-bearing lamellae could form. The cores, however, retained more Ti which facilitated supersaturation with respect to rutile or ilmenite and, thus, precipitation during retrogression. It is critical to emphasize that elements such as Ti and phosphorus (and elements involved in coupled substitutions with them including Na) only enter garnet at elevated *P-T* conditions in typical pelitic, basaltic, and ultramafic bulk compositions (e.g. Ono 1998; Hermann and Spandler 2008; Collerson et al. 2010; Konzett 2016; Ackerson et al. 2017a). As a result, there is no reason to suppose that the concentrations of such elements would *increase* during cooling and exhumation by diffusion in from the matrix. Consequently, their concentrations should be regarded as *minima*.

In view of all the foregoing evidence, we conclude that a precipitation process, in this case most likely exsolution, is the most viable explanation for the observed lamellae textures. The common theme of alternative hypotheses is that the lamellae are exogenous to the host garnet and were acquired by means of processes such as injection into garnet, co-growth of garnet and lamellae phases, or growth of garnet that traps melt or pre-existing matrix phases. For the rocks studied here, such interpretations strain credibility, as prograde and retrograde reaction histories, fluid or melt composition, matrix mineralogy, and deformation must have varied widely between localities and, as a result, a large variety of lamellae minerals would be expected. Instead, a restricted range of lamellae phases is typically observed worldwide: mostly simple oxides such as rutile, ilmenite, and srilankite, and several more chemically-complex phases, primarily apatite, pyroxene, and amphibole. By far the simplest explanation of this observation is that garnet is rejecting chemical constituents known to be stable in the garnet lattice at elevated *P*-*T* conditions, such as Ti^{4+}, P^{5+}, and pyroxene components, via exsolution during cooling and exhumation. The precipitation probably required some modest involvement of open system behavior (Proyer et al. 2013; Axler and Ague 2015a), defects (Geiger et al. 2016), or both, but essential lamellae constituents such as Ti and phosphorus were intrinsic to host garnet.

IMPLICATIONS

Crystallographic and textural evidence shows that lamellae in garnet with the traits described herein should be considered precipitates and therefore reliable petrogenetic indicators of conditions at which the necessary trace substitutions such as Ti^{4+} and P^{5+} are soluble in the garnet structure (i.e. high to ultrahigh-temperatures and pressures). Even lamellae without COR may still be precipitates, as they are commonly morphologically and texturally indistinguishable from those with COR. Silicate lamellae such as pyroxene with COR and SPO would be strong evidence of former majoritic garnet, and therefore stability at $P > \sim 5$ GPa (van Roermund and

Drury 1998; Zhang and Liou 1999; Ye et al. 2000; Dobrzhinetskaya et al. 2004; Spengler 2006; Zhang et al. 2011; Xu and Wu 2017).

Our conclusions mean that corundum can precipitate from garnet, which deserves further treatment beyond the scope of this work. As the eclogite facies metapegmatite rock hosting the Austrian garnets is quartz-saturated (Griffiths et al. 2016), it is highly implausible that corundum was emplaced or relict. We posit that breakdown of garnet with a "Ti-Tschermak" (Ackerson et al. 2017a) component can yield garnet plus ilmenite and corundum: $3Fe_3(Al,Ti)(AlSi_2)O_{12} = 2 Fe_3Al_2Si_3O_{12} + 3FeTiO_3 + Al_2O_3$. Such a reaction would be indicative of the garnet host shielding lamellae-forming reactions from the chemical influence of the quartz-saturated rock matrix.

Mineralogical COR studies began only recently, but they have great potential for studying lamellae growth, interpreting lamellae textures, and predicting lamellae crystallographic trends. Further refinement of quantitative methods for comparing and predicting COR will illuminate the micro- and nanoscale processes governing lamellae formation, and in doing so, guide mineralogical and petrological interpretations of lamellae textures, including the use of COR as petrogenetic indicators.

ACKNOWLEDGMENTS

We thank J. A. Axler, S. Nicolescu, D. M. Rye, E. M. Stewart, M. T. Brandon, D. A. D. Evans, and S. Ferrero for discussions, Z. Jiang for EBSD assistance, T. A. Griffiths for helpful discussions on interpreting the datasets of Griffiths et al. (2016), and M. R. Ackerson and A. Putnis for thorough and constructive reviews. This work was supported by the US National Science Foundation Directorate of Geosciences (EAR-0744154, EAR-1250269, and EAR-1753553) and Yale University.

References

Ackerson, M.R., Watson, E.B., Tailby, N.D. and Spear, F.S. (2017) Experimental investigation into the substitution mechanisms and solubility of Ti in garnet. American Mineralogist, 102, 158–172.

Ackerson, M.R., Tailby, N.D. and Watson, E.B. (2017) XAFS spectroscopic study of Ti coordination in garnet. American Mineralogist, 102, 173–183.

Ague, J.J. and Eckert, J.O. Jr. (2012) Precipitation of rutile and ilmenite needles in garnet: Implications for extreme metamorphic conditions in the Acadian Orogen, U.S.A. American Mineralogist, 97, 840–855.

Ague, J.J., Eckert, J.O. Jr., Chu, X., Baxter, E.F. and Chamberlain, C.P. (2013) Discovery of ultrahigh-temperature metamorphism in the Acadian orogen, Connecticut, USA. Geology, 41, 271–274.

Ague, J.J. and Axler, J.A. (2016) Interface coupled dissolution-reprecipitation in garnet from subducted granulites and ultrahigh-pressure rocks revealed by phosphorous, sodium, and titanium zonation. American Mineralogist, 101, 1696–1699.

Alifirova, T.A., Pokhilenko, L.N. and Korsakov, A.V. (2015) Apatite, SiO_2, rutile and orthopyroxene precipitates in minerals of eclogite xenoliths from Yakutian kimberlites, Russia. Lithos, 226, 31–49.

Åmli, R. (1975) Mineralogy and Rare Earth Geochemistry of Apatite and Xenotime from the Gloserheia Granite Pegmatite, Froland, Southern Norway. American Mineralogist, 60, 607–620.

Andersson, S. and O'Keeffe, M. (1977) Body-centered cubic cylinder packing and the garnet structure. Nature, 267, 605–606.

Auzanneau, E., Schmidt, M.W., Vielzeuf, D. and Connolly, J.A.D. (2010) Titanium in phengite: a geobarometer for high temperature eclogites. Contributions to Mineralogy and Petrology, 159, 1–24.

Axler, J.A. and Ague, J.J. (2015a) Exsolution of rutile or apatite precipitates surrounding ruptured inclusions in garnet from UHT and UHP rocks. Journal of Metamorphic Geology, 33, 829–848.

Axler, J.A. and Ague, J.J. (2015b) Oriented multiphase needles in garnet from ultrahigh-temperature granulites, Connecticut, U.S.A. American Mineralogist, 100, 2254–2271.

Bachmann, F., Hielscher, R. and Schaeben, H. (2010) Texture Analysis with MTEX – Free and Open Source Software Toolbox. Solid State Phenomena, 160, 63–68.

Balluffi, R.W., Allen, S.M. and Carter, W.C. (2005) Kinetics of Materials, 645 p. Wiley, Hoboken.

Baumann, S.F., Michael, J. and Williams, D.B. (1981) Initiation and Growth of the Grain Boundary Discontinuous Precipitation Reaction. Acta Metallurgica, 29, 1343–1355.

Boudeulle, M. (1994) Disproportionation in Mineral Solid Solutions: Symmetry Constraints on Precipitate Orientation and Morphology. Implications for the Study of Oriented Intergrowths. Journal of Applied Crystallography, 27, 567–573.

Brandon, D.G. (1966) The structure of high-angle grain boundaries. Acta Metallurgica, 14, 1479–1484.

Brunet, F., Allan, D.R., Redfern, S.A.T., Angel, R.J., Miletich, R., Reichmann, H.J., Sergent, J. and Hanfland, M. (1999) Compressibility and thermal expansivity of synthetic apatites, $Ca_5(PO_4)_3X$ with W = OH, F and Cl. European Journal of Mineralogy, 11, 1,023–1,035.

Bunge, J.H., Weiss, W., Klein, H., Wcislak, L., Garbe, U. and Schneider, J.R. (2003) Orientation relationship of Widmanstätten plates in an iron meteorite measured with high-energy synchrotron radiation. Journal of Applied Crystallography, 36, 137–140.

Cahn, J.W. (1957) Nucleation on Dislocations. Acta Metallurgica, 5, 169–172.

Cahn, J.W. and Hilliard, J.E. (1971) Spinodal Decomposition: A Reprise. Acta Metallurgica, 19, 151–161.

Cahn, J.W., Pan, J.D. and Balluffi, R.W. (1979) Diffusion Induced Grain Boundary Migration. Scripta Metallurgica, 13, 503–509.

Cayron, C. (2014) EBSD imaging of orientation relationships and variant groupings in different martensitic alloys and Widmanstätten iron meteorites. Materials Characterization, 94, 93–110.

Chakraborty, S. and Ganguly, J. (1992) Cation diffusion in aluminosilicate garnets: experimental determination in spessartine-almandine diffusion couples, evaluation of effective binary diffusion coefficients, and applications. Contributions to Mineralogy and Petrology, 111, 74–86.

Chu, X. and Ague, J.J. (2015) Analysis of experimental data on divalent cation diffusion kinetics in aluminosilicate garnets with application to timescales of peak Barrovian metamorphism, Scotland. Contributions to Mineralogy and Petrology, 170:25.

Colasanti, C.V., Johnson, E.A. and Manning, C.E. (2011) An experimental study of OH solubility in rutile at 500–900 °C, 0.5–2 GPa, and a range of oxygen fugacities. American Mineralogist, 96, 1291–1299.

Collerson, K.D., Williams, Q., Kamber, B.S., Omori, S., Hiroyoshi, A. and Ohtani, E. (2010) Majoritic garnet: A new approach to pressure estimation of shock events in meteorites and the encapsulation of sub-lithospheric inclusions in diamond. Geochimica et Cosmochimica Acta, 74, 5939–5957.

Daneu, N., Rečnik, A. and Mader, W. (2014) Atomic structure and formation mechanism of (101) rutile twins from Diamantina (Brazil). American Mineralogist, 99, 612–624.

Dobrzhinetskaya, L.F., Green, H.W. II, Renfro, A.P., Bozhilov, K.N., Spengler, D. and van Roermund, H.R.M. (2004) Precipitation of pyroxenes and Mg_2SiO_4 from majoritic garnet: simulation of peridotite exhumation from great depth. Terra Nova, 16, 325–330.

Escudero, A., Langenhorst, F. and Müller, W.F. (2012) Aluminum solubility in TiO_2 rutile at high pressure and experimental evidence for a $CaCl_2$-structured polymorph. American Mineralogist, 97, 1075–1082.

Fiquet, G., Richet, P. and Montagnac, G. (1999) High-temperature thermal expansion of lime, periclase, corundum and spinel. Physics and Chemistry of Minerals, 27, 103–111.

Fisher, J.C., Hollomon J.H. and Leschen, J.G. (1952) Precipitation from Solid Solution. Industrial and Engineering Chemistry, 44, 1324–1327.

Fujii, T., Tohgo, K., Mori, Y. and Shimamura, Y. (2018) Crystallography of intergranular corrosion in sensitized austentitic stainless steel. Materials Characterization, 144, 219–226.

Fung, A. and Haggerty, S.E. (1995) Petrography and mineral compositions of eclogites from the Koidu Kimberlite Complex, Sierra Leone. Journal of Geophysical Research, 100, 20,451–20,473.

Geiger, C.A., Brearley, A.J., Dachs, E., Tipplet, G. and Rossman, G.R. (2016) A Study of Defect Behavior in Almandine Garnet. AGU Abstracts with Programs, MR42A-03.

Goldstein, J.I. and Ogilvie, R.E. (1965) The growth of the Widmanstätten pattern in metallic meteorites. Geochimica et Cosmochimica Acta, 29, 893–920.

Griffin, W. L., Jensen, B.B. and Misra, S.N. (1971) Anomalously elongated rutile in eclogite-facies pyroxene and garnet. Norsk Geologisk Tidsskrift, 51, 177–185.

Griffin, W.L. (2008) Major transformations reveal Earth's deep secrets. Geology, 36, 95–96.

Griffiths, T.A., Habler, G. and Abart, R. (2016) Crystallographic orientation relationships in host–inclusion systems: New insights from large EBSD data sets. American Mineralogist, 101, 690–705.

Griffiths, T.A., Habler, G., Schantl, P. and Abart, R. (2017) Crystallographic Orientation Relationships (CORs) between rutile inclusions and garnet hosts: towards using COR frequencies as a petrogenetic indicator. Geophysical Research Abstracts, 19, EGU2017-7523.

Habler, G. and Griffiths, T. (2017) Crystallographic orientation relationships, *in* Heinrich, W. and Abart, R., eds., Mineral reaction kinetics: Microstructures, textures, chemical and isotopic signatures. European Mineralogical Union Notes in Mineralogy, 16, 541–585.

Hacker, B.R., Sharp, T., Zhang, R.Y., Liou, J.G. and Hervig, R.L. (1997) Determining the Origin of Ultrahigh-Pressure Lherzolites. Science, 278, 702–704.

Hammer, J.E., Sharp, T.G. and Wessel, P. (2010) Heterogeneous nucleation and epitaxial crystal growth of magmatic minerals. Geology, 38, 367–370.

Harlov, D.E., Wirth, R. and Förster, H.J. (2005) An experimental study of dissolution-reprecipitation in fluorapatite: fluid infiltration and the formation of monazite. Contributions to Mineralogy and Petrology, 150, 268–286.

Harte, B. (2010) Diamond formation in the deep mantle: the record of mineral inclusions and their distribution in relation to mantle dehydration zones. Mineralogical Magazine, 74, 189–215.

He, Y., Godet, S. and Jonas, J.J. (2006) Observations of the Gibeon meteorite and the inverse Greninger-Troiano orientation relationship. Journal of Applied Crystallography, 39, 72–81.

Hermann, J. and Spandler, C.J. (2008) Sediment Melts at Sub-arc Depths: an Experimental Study. Journal of Petrology, 49, 717–740.

Hielscher, R., Schaeben, H. and Siemes, H. (2010) Orientation Distribution Within a Single Hematite Crystal. Mathematical Geosciences, 42, 359–375.

Howe, J.M. (1997) Interfaces in Materials: Atomic Structure, Thermodynamics and Kinetics of Solid-Vapor, Solid-Liquid and Solid-Solid Interfaces, 516 p. Wiley, New York.

Hutchinson, B., Ryde, L. and Bate, P. (2005) Transformation Textures in Steels. Materials Science Forum, 495-497, 1141–1150.

Hwang, S.L., Yui, T.F., Chu, H.T., Shen, P., Schertl, H.P., Zhang, R.Y. and Liou, J.G. (2007) On the origin of oriented rutile needles in garnet from UHP eclogites. Journal of Metamorphic Geology, 25, 349–362.

Hwang, S.L., Shen, P., Chu, H.T., Yui, T.F. and Iizuka, Y. (2015) Origin of rutile needles in star garnet and implications for interpretation of inclusion textures in ultrahigh-pressure metamorphic rocks. Journal of Metamorphic Geology, 33, 249–272.

Hwang, S.L., Shen, P., Chu, H.T. and Yui, T.F. (2016) On the forbidden and the optimum crystallographic variant of rutile in garnet. Journal of Applied Crystallography, 49, 1922–1940.

Keller, D.S. and Ague, J.J. (2018) High-pressure granulite facies metamorphism (~1.8 GPa) revealed in silica-undersaturated garnet-spinel-corundum gneiss, Central Maine Terrane, Connecticut, U.S.A. American Mineralogist, 103, 1851-1868.

Konzett, J. (2016) From phosphates to silicates and back: An experimental study on the transport and storage of phosphorus in eclogites during uplift and exhumation. American Mineralogist, 101, 1756–1768.

Liu, S.J., Li, J.H. and Santosh, M. (2010) First application of the revised Ti-in-zircon geothermometer to Paleoproterozoic ultrahigh-temperature granulites of Tuguiwula, Inner Mongolia, North China Craton. Contributions to Mineralogy and Petrology, 159:225–235.

Marquardt, K., Rohrer, G.S., Morales, L., Rybacki, E., Marquardt, H. and Lin, B. (2015) The most frequent interfaces in olivine aggregates: the GBCD and its importance for grain boundary related processes. Contributions to Mineralogy and Petrology, 170:40.

Meagher, E.P. and Lager, G.A. (1979) Polyhedral thermal expansion in the TiO_2 Polymorphs: Refinement of the Crystal Structures of Rutile and Brookite at High Temperature. Canadian Mineralogist, 17, 77–85.

Morito, S., Huang, X., Furuhara, T., Maki, T. and Hansen, N. (2006) The morphology and crystallography of lath martensite in alloy steels. Acta Materialia, 54, 5323–5331.

Mposkos, E.D. and Kostopoulos, D.K. (2001) Diamond, former coesite and supersilicic garnet in metasedimentary rocks from the Greek Rhodope: a new ultrahigh-pressure metamorphic province established. Earth and Planetary Science Letters, 192, 497–506.

Nabarro, F.R.N. (1940) The Strains Produced by Precipitation in Alloys. Proceedings of the Royal Society of London A, 175, 519–538.

O'Brien, P.J. (2008) Challenges in high-pressure granulite metamorphism in the era of pseudosections: reaction textures, compositional zoning and tectonic interpretation with examples from the Bohemian Massif. Journal of Metamorphic Geology, 26, 235–251.

Ono, S. (1998) Stability limits of hydrous minerals in sediment and mid-ocean ridge basalt compositions: Implications for water transport in subduction zones. Journal of Geophysical Research, 103, 18253–18267.

Perchuk, A.L. (2008) Unusual Inclusions in Garnet from the Diamond-Bearing Gneiss of the Erzgebirge, Germany. Geochemistry International, 46, 296–303.

Phillips, D.S., Heuer, A.H. and Mitchell, T.E. (1980) Precipitation in star sapphire I. Identification of the precipitate. Philosophical Magazine A, 42, 385–404.

Pollok, K., Lloyd, G.E., Austrheim, H. and Putnis, A. (2008) Complex replacement patterns in garnets from Bergen Arcs eclogites: A combined EBSD and analytical TEM study. Chemie der Erde, 68, 177–191.

Proyer, A., Krenn, K. and Hoinkes, G. (2009) Oriented precipitates of quartz and amphibole in clinopyroxene of metabasites from the Greek Rhodope: a product of open system precipitation during eclogite–granulite–amphibolite transition. Journal of Metamorphic Geology, 27, 639–654.

Proyer, A., Habler, G., Abart, R., Wirth, R., Krenn, K. and Hoinkes, G. (2013) TiO_2 exsolution from garnet by open-system precipitation: evidence from crystallographic and shape preferred orientation of rutile inclusions. Contributions to Mineralogy and Petrology, 166, 211–234.

Putnis, A. (1992) An Introduction to Mineral Sciences, 457 p. Cambridge University Press, New York.

Putnis A. and John T. (2010) Replacement processes in the Earth's crust. Elements, 6, 159–164.

Qian, Q. and Hermann, J. (2013) Partial melting of lower crust at 10–15 kbar: constraints on adakite and TTG formation. Contributions to Mineralogy and Petrology, 165, 1195–1224.

Ramsden, A.R. and Cameron, E.N. (1966) Kamacite and taenite superstructures and a metastable tetragonal phase in iron meteorites. American Mineralogist, 51, 37–55.

Rečnik, A., Stanković, N. and Daneu, N. (2015) Topotaxial reactions during the genesis of oriented rutile/hematite intergrowths from Mwinilunga (Zambia). Contributions to Mineralogy and Petrology, 169:19.

Ringwood, A.E. and Major, A. (1971) Synthesis of majorite and other high pressure garnets and perovskites. Earth Planetary Science Letters, 12, 411–418.

Rohrer, G.S. (2011) Grain boundary energy anisotropy: a review. Journal of Materials Science, 46, 5881–5895.

Ruiz-Cruz, M.D. and Sanz de Galdeano, C. (2013) Coesite and diamond inclusions, exsolution microstructures and chemical patterns in ultrahigh pressure garnet from Ceuta (Northern Rif, Spain). Lithos, 177, 184–206.

Sakamaki, K., Sato, Y. and Ogasawara, Y. (2016) Hydrous Na-garnet from Garnet Ridge; products of mantle metasomatism underneath the Colorado Plateau. Progress in Earth and Planetary Science, 3:20.

Sánchez-Muñoz, L., del Campo, A. and Fernández, J.F. (2016) Symmetry constraints during the development of anisotropic spinodal patterns. Scientific Reports, 6:20806.

Santoro, A. and Mighell, A.D. (1973) Coincidence-Site Lattices. Acta Crystallographica, A29, 169–175.

Shiflet, G.J. and van der Merwe, J.H. (1994) The Role of Structural Ledges as Misfit-Compensating Defects: fcc-bcc Interphase Boundaries. Metallurgical and Materials Transactions A, 25A, 1895–1903.

Sobolev, N.V. Jr. and Lavrent'ev, J.G. (1971) Isomorphic Sodium Admixture in Garnets Formed at High Pressures. Contributions to Mineralogy and Petrology, 31, 1–12.

Sonderegger, B., Mitsche, S. and Cerjak, H. (2007) Martensite laths in creep resistant martensitic 9–12% Cr steels — Calculation and measurement of misorientations. Materials Characterization, 58, 874–882.

Song, S., Zhang, L., Chen, J., Liou, J.G. and Niu, Y. (2005) Sodic amphibole exsolutions in garnet from garnet-peridotite, North Qaidam UHPM belt, NW China: Implications for ultradeep-origin and hydroxyl defects in mantle garnets. American Mineralogist, 90, 814–820.

Spengler, D. (2006) Origin and Evolution of Deep Upper Mantle Rocks from Western Norway [Ph.D. Thesis]. University of Utrecht, 287 p.

Stanford, N. and Bate, P.S. (2005) Crystallographic variant selection in α–β brass. Acta Materialia, 53, 859–867.

Tan, W., He, H., Yan Wang, C. Dong, H., Liang, X. and Zhu, J. (2016) Magnetite exsolution in ilmenite from the Fe-Ti oxide gabbro in the Xinjie intrusion (SW China) and sources of unusually strong remnant magnetization. American Mineralogist, 101, 2759–2767.

Thiéblot, L., Roux, J. and Richet, P. (1998) High-temperature thermal expansion and decomposition of garnets. European Journal of Mineralogy, 10, 7–15.

van Roermund, H.L.M. and Drury, M.R. (1998) Ultra-high pressure (P > 6 GPa) garnet peridotites in Western Norway: exhumation of mantle rocks from > 185 km depth. Terra Nova, 10, 295–301.

van Roermund, H.L.M., Drury, M.R., Barnhoorn, A. and de Ronde, A. (2000) Non-silicate inclusions in garnet from an ultra-deep orogenic peridotite. Geological Journal, 35, 209–229.

Voss, D.A., Butler, E.P. and Mitchell, T.E. (1982) The Growth of Hematite Blades during the High Temperature Oxidation of Iron. Metallurgical and Materials Transactions A, 13A, 929–935.

Wang, L., Essene, E.J. and Zhang, Y. (1999) Mineral inclusions in pyrope crystals from Garnet Ridge, Arizona, USA: implications for processes in the upper mantle. Contributions to Mineralogy and Petrology, 135, 164–178.

Wechsler, B.A. and Prewitt, C.T. (1984) Crystal structure of ilmenite ($FeTiO_3$) at high temperature and at high pressure. American Mineralogist, 69, 176–185.

Wenk, H.R., Chen, K. and Smith, R. (2011) Morphology and microstructure of magnetite and ilmenite inclusions in plagioclase from Adirondack anorthositic gneiss. American Mineralogist, 96, 1316–1324.

Wijbrans, C.H., Rohrbach, A. and Klemme, S. (2016) An experimental investigation of the stability of majoritic garnet in the Earth's mantle and an improved majorite geobarometer. Contributions to Mineralogy and Petrology, 171:50.

Wood, B.J., Kiseeva, E.S. and Matzen, A.K. (2013) Garnet in the Earth's Mantle. Elements, 9, 421–426.

Xu, H.J. and Wu, Y. (2017) Oriented inclusions of pyroxene, amphibole, and rutile in garnet from the Lüliangshan garnet peridotite massif, North Qaidam UHPM belt, NW China: an electron backscatter diffraction study. Journal of Metamorphic Geology, 35, 1–17.

Ye, K., Cong, B. and Ye, D. (2000) The possible subduction of continental material to depths greater than 200 km. Nature, 407, 734–736.

Zack, T., Moraes, R. and Kronz, A. (2004) Temperature dependence of Zr in rutile: empirical calibration of a rutile thermometer. Contributions to Mineralogy and Petrology, 148, 471–488.

Zhang, J.F., Xu, H.J., Liu, Q., Green, H.W. II and Dobrzhinetskaya, L.F. (2011) Pyroxene exsolution topotaxy in majoritic garnet from 250 to 300 km depth. Journal of Metamorphic Geology, 29, 741–751.

Zhang, R.Y. and Liou, J.G. (1999) Exsolution Lamellae in Minerals from Ultrahigh-Pressure Rocks. International Geology Review, 41, 981–993.

Zhao, J., Brugger, J., Grguric, B.A., Ngothai, Y. and Pring, A. (2017) Fluid-Enhanced Coarsening of Mineral Microstructures in Hydrothermally Synthesized Bornite-Digenite Solid Solution. ACS Earth and Space Chemistry, 1, 465–474.

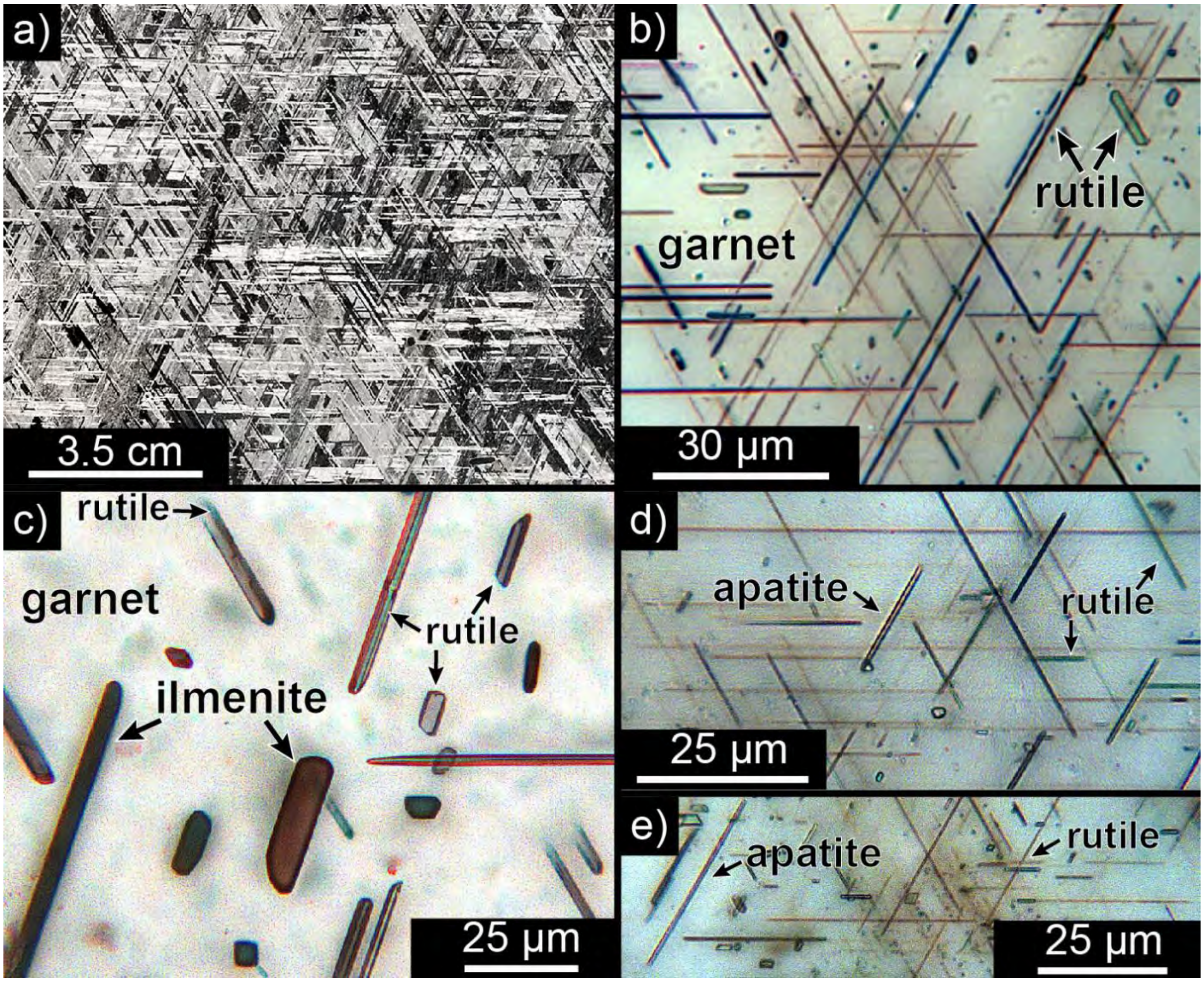

FIGURE 1: Precipitation structures in natural samples. **a)** Widmanstätten pattern in the Gibeon meteorite (photo courtesy of Christie's). **b)** Thin section photomicrograph of rutile oriented along <111>$_{\text{garnet}}$ from the Brimfield Schist, CT (341B-5). **c)** Thin section photomicrograph of rutile and ilmenite needles and plates in garnet from the Brimfield Schist, CT (322A-1). **d)** and **e)** rutile and apatite lamellae (341B-5). Extended depth of field maintains focus throughout the depth of the thin sections in panels **b)** through **e)** (see Methods).

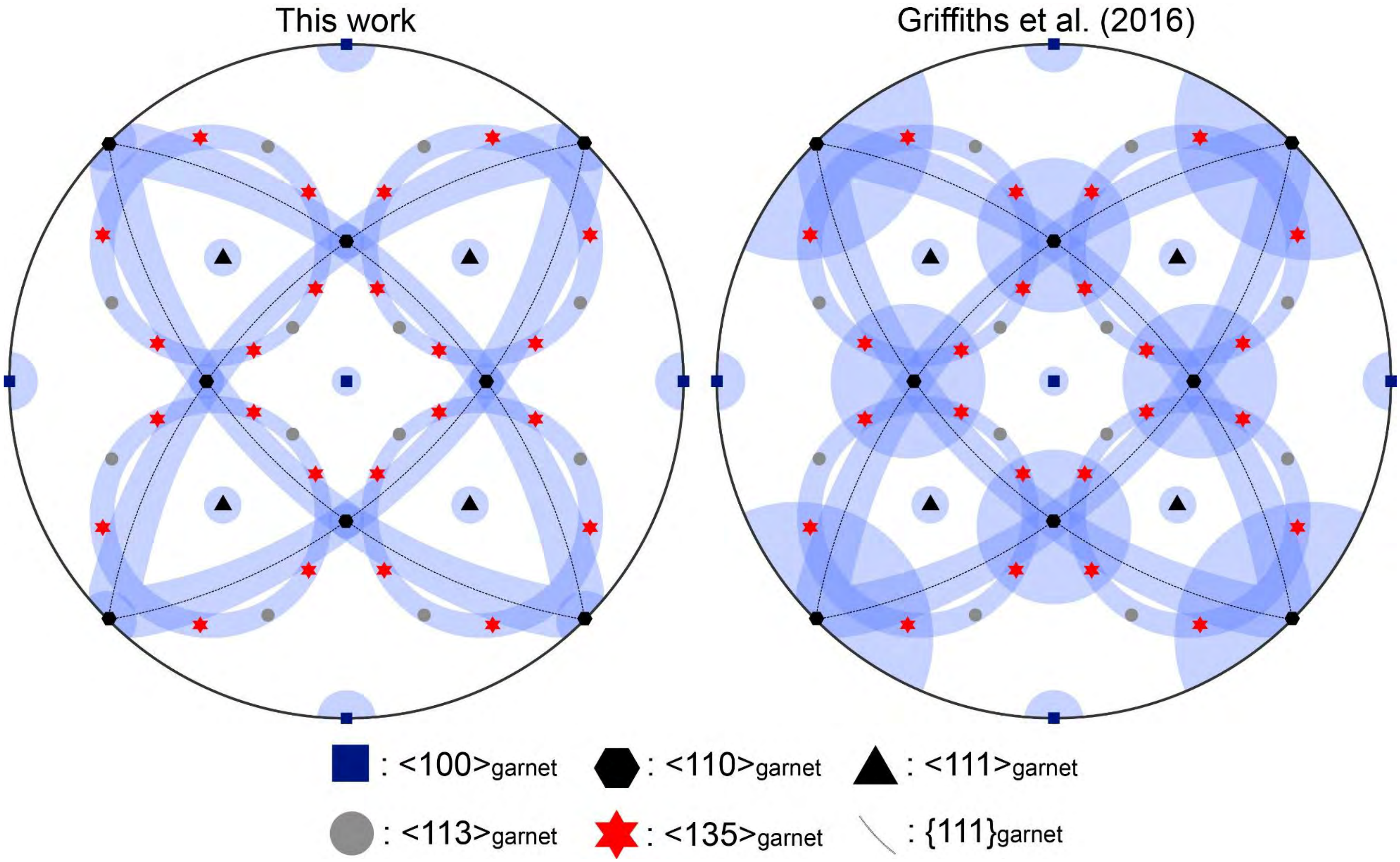

FIGURE 2: Equal-angle stereographic projections showing angular COR search criteria used in this work and that of Griffiths et al. (2016).

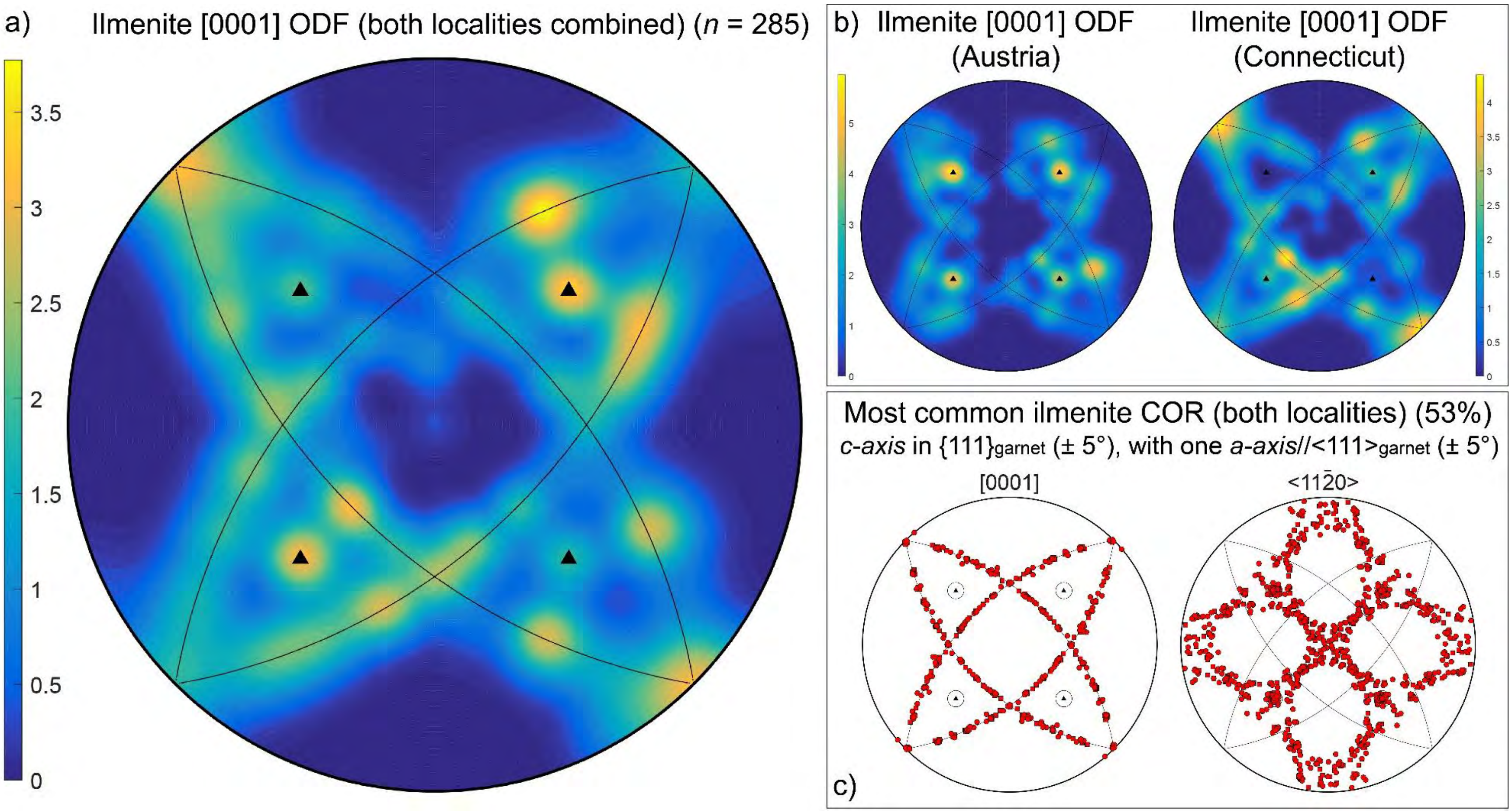

FIGURE 3: Statistical distributions of ilmenite COR. **a)** Orientation distribution function (ODF) of all ilmenite *c-axes* in garnet from the CT and Austria samples. **b)** ODFs for the CT and Austria localities. Colorbars show multiples of a random distribution (MRD). Each plot includes all analyzed data from each locality rotated into the same frame of reference. Garnet {111} (lines) and <111> (triangles) are plotted for reference. **c)** Upper hemisphere, symmetrized, equal angle stereographic projections show position of ilmenite axes for the most prevalent COR.

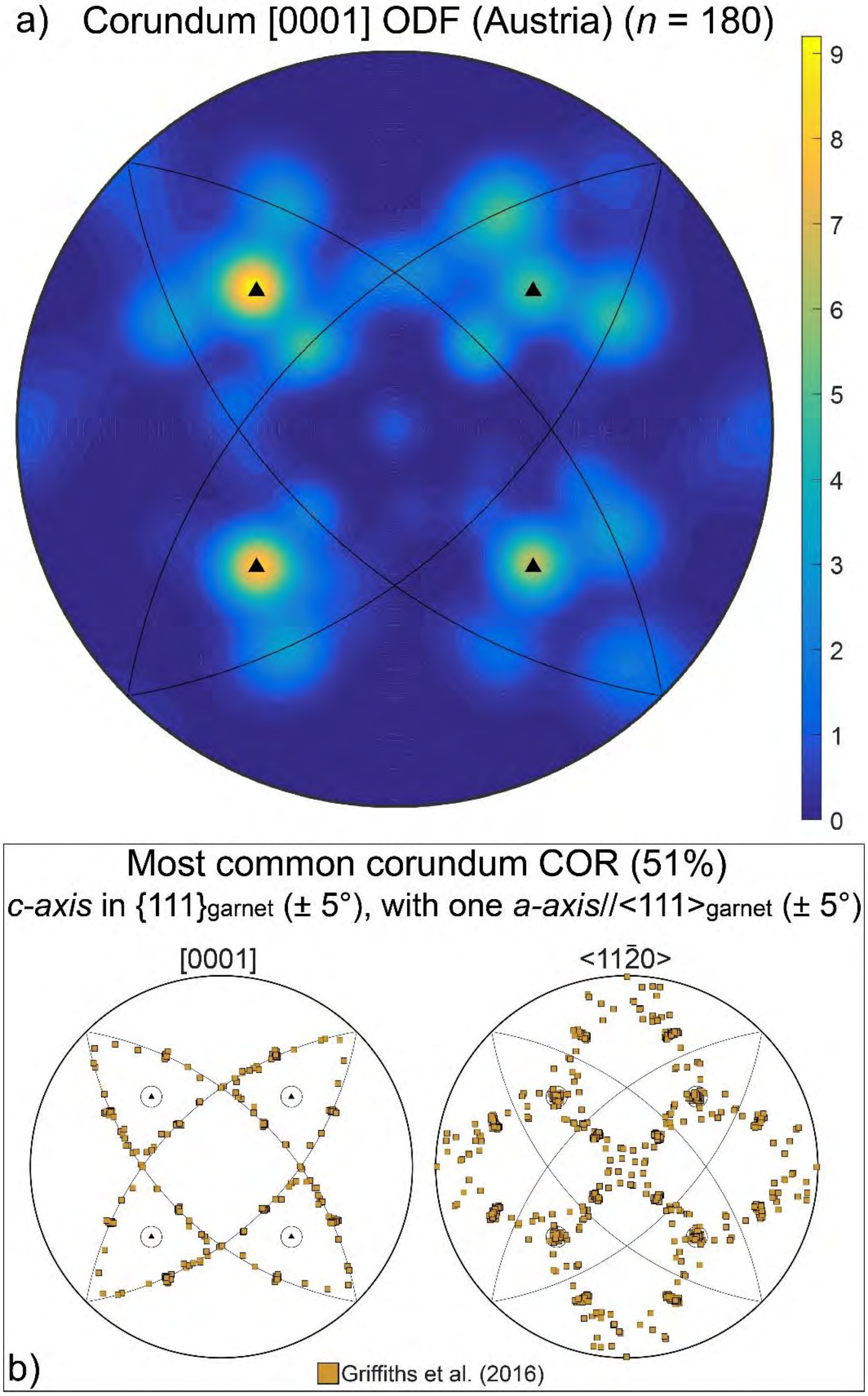

FIGURE 4: Statistical distribution of corundum COR. **a)** Orientation distribution function (ODF) of all corundum *c-axes* in garnet from the Austria samples. Colorbar shows multiples of a random distribution (MRD). Garnet {111} (lines) and <111> (triangles) are plotted for reference. **b)** Upper hemisphere, symmetrized, equal angle stereographic projections show position of corundum axes for the most prevalent COR.

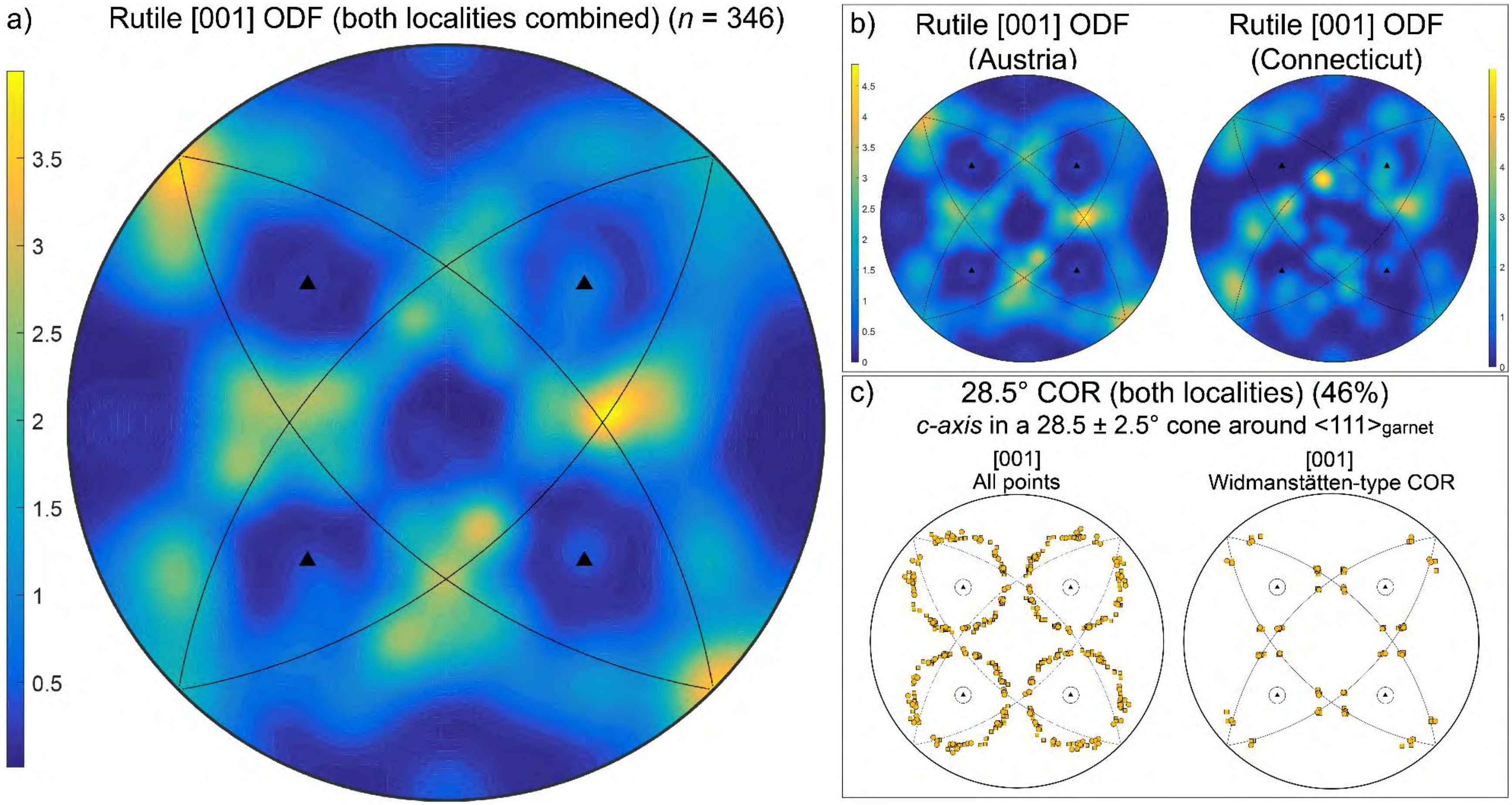

FIGURE 5: Statistical distributions of rutile COR. **a)** Orientation distribution function (ODF) of all rutile *c-axes* in garnet from the CT and Austria samples. **b)** ODFs for the CT and Austria localities. Colorbars show multiples of a random distribution (MRD). Each plot includes all analyzed data from each locality rotated into the same frame of reference. Garnet {111} (lines) and <111> (triangles) are plotted for reference. **c)** Upper hemisphere, symmetrized, equal angle stereographic projections show position of rutile *c-axes* for the 28.5° COR and its specific subgroup the Widmanstätten-type COR.

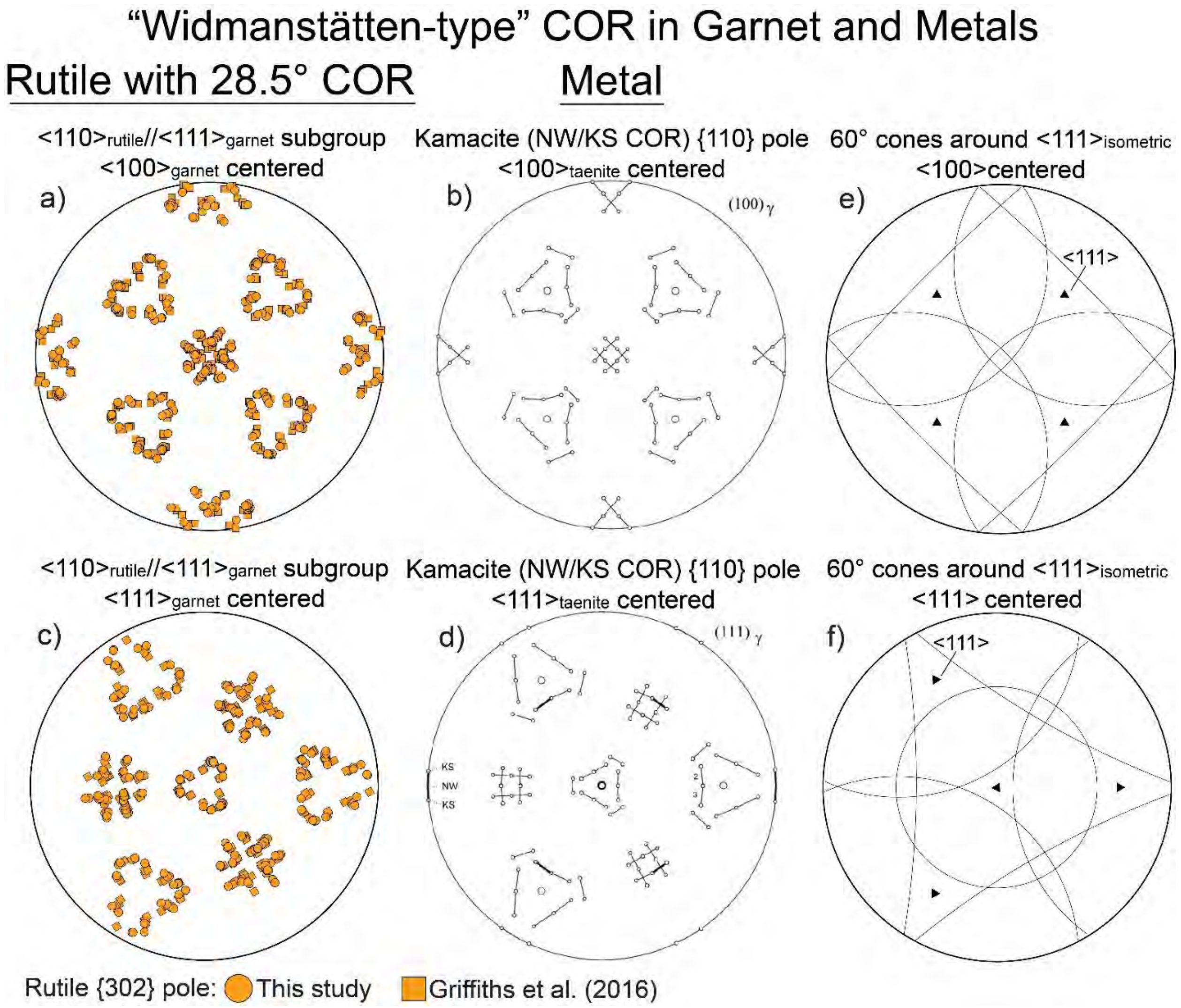

FIGURE 6: Widmanstätten-type COR for rutile in garnet compared to metals (symmetrized plots). **a)** For rutile with *c-axis* in $\{111\}_{\mathrm{garnet}}$ and $<110>//<111>_{\mathrm{garnet}}$, poles to $\{302\}_{\mathrm{rutile}}$ trace the NW-KS COR. **b)** Calculated NW-KS CORs in meteoritic nickel-iron after Bunge et al. (2003). Panels **c)** and **d)** are the same data as panels **a)** and **b)** rotated to a 3-fold frame of reference. **e), f)** 60° cones around $<111>_{\mathrm{garnet}}$ for comparison with parts a)–d).

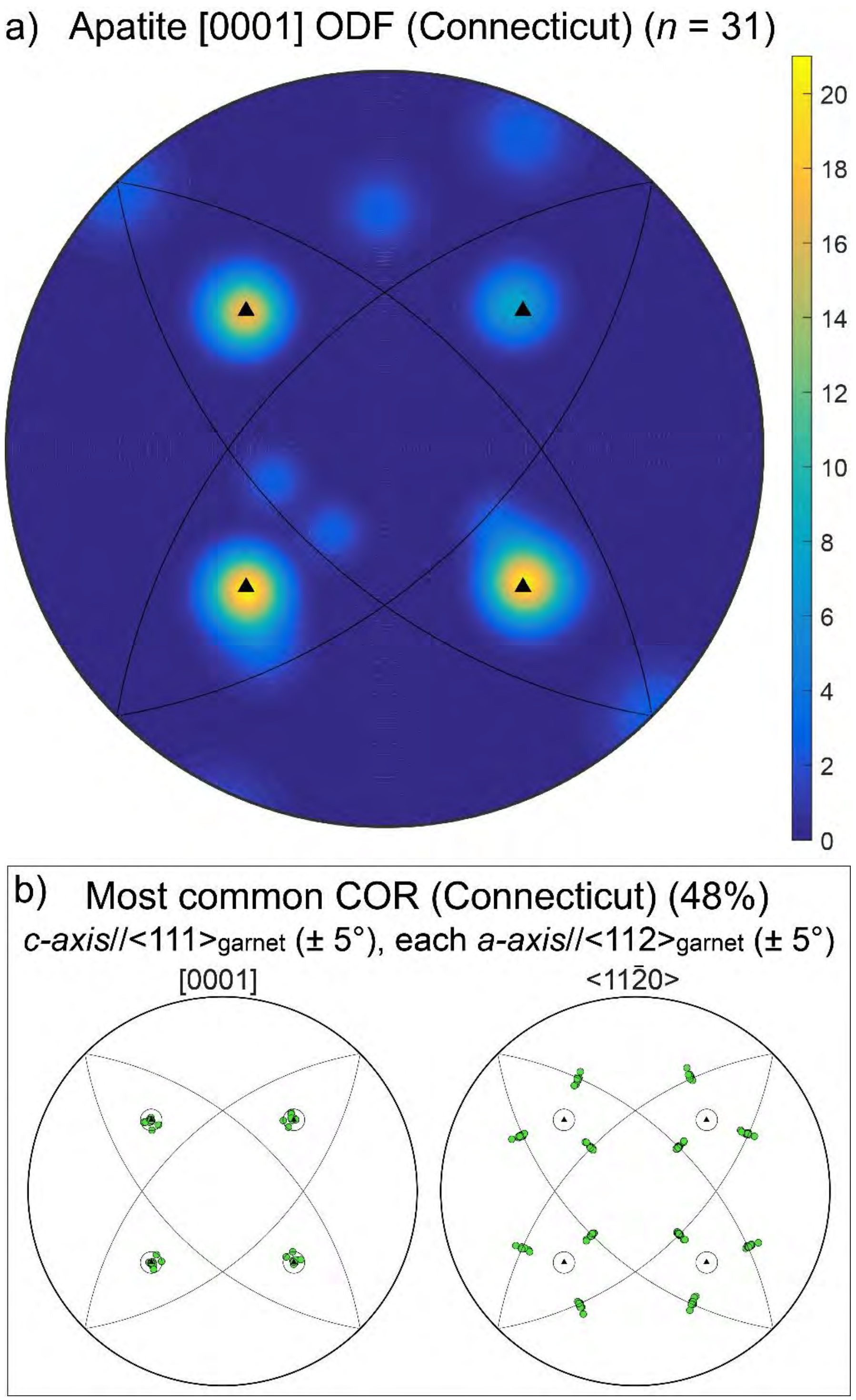

FIGURE 7: Statistical distribution of apatite COR. **a**) Orientation distribution function (ODF) of all apatite *c-axes* in garnet from the CT samples. Colorbar shows multiples of a random distribution (MRD). The plot includes all analyzed data rotated into the same frame of reference. Garnet {111} (lines) and <111> (triangles) are plotted for reference. **b)** Upper hemisphere, symmetrized, equal angle stereographic projections show position of apatite axes for the most prevalent COR.

Table 1: Some hypotheses for lamellae formation in garnet with brief commentary

Hypothesis	Predicted Textures	Predicted SPO	COR	Comments	Status
Precipitation (e.g. Exsolution)	Three-dimensional, consistent distribution of lamellae within the host garnet	Garnet axes or planes	Predicted and observed	• Likely produces inclined extinction in rutile[1,2] • OSP may be needed to explain substitutions in garnet for minerals such as rutile[1,3]	Viable
Growth during ICDR	Lamellae, possibly uniformly distributed, in recrystallized zones of host garnet	Garnet axes or planes	Unconfirmed	• Reaction fronts likely to be preserved and observable in electron backscatter images and/or chemical maps[4,5] • Asymmetrical distribution of lamellae could reveal a reaction front • Not yet shown to produce COR	Plausible
Co-growth of garnet and lamellae	Garnet with protruding oxide lamellae or lamellae flat on or terminating at faces	Tied to fast growth directions	Unconfirmed (no epitaxy w/ garnet yet established)	• No reports of garnet with protruding oriented oxide lamellae, nor those lying flat on garnet faces, nor terminating exactly at faces • Not produced in laboratory experiments • Lamellae expected to be minerals in equilibrium with rock matrix; this is not always observed	Implausible
Etching of garnet and deposition of lamellae, followed by overgrowth	Lamellae along host planes, likely unevenly distributed	Garnet planes	Unconfirmed (no epitaxy w/ garnet yet established)	• Expected to produce a high proportion of lamellae without axial SPO • Expected to produce at least some interconnected lamellae networks	Implausible
Overgrowth of pre-existing crystals	Uneven distribution of lamellae	Random or interpenetrating networks	Unconfirmed	• Many lamellae show growth habits not observed in matrix examples • No reason for overgrown lamellae to be restricted to $<111>_{garnet}$ or oriented in three-dimensional arrays in the rock matrix	Rejected
Cleaving and fluid or melt emplacement into garnet	Lamellae along host planes and planar junctions, likely unevenly distributed	Garnet planes and axes	Unconfirmed in garnet	• Garnet lacks cleavage • Lamellae expected to be minerals in equilibrium with rock matrix; this is not always observed • No known crustal fluids precipitate only oxides • Fluid pockets at lamellae edges not conclusive evidence of emplacement as lamellae or host garnet may exsolve H_2O during retrogression	Rejected

Notes: OSP – open-system precipitation; SPO – shape-preferred orientation; COR – crystallographic orientation relationship; ICDR – interface-coupled dissolution-reprecipitation. [1]Proyer et al. (2013) [2]Phillips et al. 1980 [3]Proyer et al. (2009, 2013) [4]Harlov et al. (2005) [5]Keller and Ague (2018). See text for additional discussion.

Table 2: COR distributions of hexagonal and trigonal lamellae measured by EBSD

	CT (This study)		Austria (Griffiths et al. 2016)		COR Type	Corresponding COR in Other Work
	Apatite	Ilmenite	Ilmenite	Corundum		
Total Measured	31	187	100	180		
COR classifications						
c-axis in $\{111\}_{garnet}$ (± 5°), with one *a-axis*//$<111>_{garnet}$ (± 5°)	6%	53%	54%	51%	Rotational Statistical*	I3,C4[1]
c-axis in $\{111\}_{garnet}$ (± 5°), with one $<10\bar{1}0>$//$<111>_{garnet}$ (± 5°)	n.o.	17%	4%	3%	Rotational Statistical*	
c-axis in $\{111\}_{garnet}$ (± 5°) only	6%	10%	6%	6%	Statistical	
***c-axis*//$<111>_{garnet}$ (± 5°), with $<10\bar{1}0>$//$<110>_{garnet}$**	48%	2%	20%	29%	Specific	I2a,C2a[1]
c-axis//$<111>_{garnet}$ (± 5°)	23%	3%	1%	2%	Statistical	I2,C2[1]
c-axis in 28.5° ± 2.5° cone around $<111>_{garnet}$	3%	2%	6%	1%	Rotational Statistical	
c-axis//$<100>_{garnet}$ (± 5°)	n.o.	<1%	n.o.	2%	Statistical	C3[1]
Total percentage with COR	***87%***	***88%***	***91%***	***94%***		
No fit assigned	13%	12%	9%	6%		CX/IX[1]

Notes: n.o. = not observed. **Bolded** COR correspond to those with low strain indicated in Table 4. See Methods for discussion of COR category determination. Total percentages of ilmenite and corundum lamellae with COR using the Griffiths et al. (2016) classification are 96%. COR types are from Habler and Griffiths (2017). [1]Griffiths et al. (2016). *Specific COR may be distinguished within this statistical COR, see Supplemental Table S2.

Table 3: Prevalence of different COR for rutile lamellae in garnet, measured by EBSD

	CT (This study)	Austria (Griffiths et al. 2016)	COR Type	Corresponding COR in Other Work
	Rutile	Rutile		
Total Measured	96	250		
<u>COR classifications</u>				
c-axis in 28.5° ± 2.5° cone around $\langle 111\rangle_{garnet}$ ($\langle 103\rangle_{rutile}$//$\langle 111\rangle_{garnet}$)	35%	34%	Rotational Statistical	R3[2]
***c-axis* in 28.5° ± 2.5° cone around $\langle 111\rangle_{garnet}$, with $\langle 110\rangle_{rutile}$//$\langle 111\rangle_{garnet}$ (± 5°); Widmanstätten-type COR**	20%	8%	Specific	COR-2[1]
c-axis//$\langle 110\rangle_{garnet}$ (± 5°)	5%	17%	Statistical	R1[1,2]
c-axis//$\{111\}_{garnet}$, with *a-axis*//$\langle 111\rangle_{garnet}$ (± 5°)	3%	10%	Rotational Statistical	
c-axis in $\{111\}_{garnet}$ (± 5°) only	5%	5%	Statistical	
c-axis//$\langle 111\rangle_{garnet}$ (± 5°)	3%	2%	Statistical	COR-4/4b[1], R2
c-axis//$\langle 100\rangle_{garnet}$ (± 5°)	1%	<1%	Statistical	COR-5/5b[1]
<u>Total percentage with COR</u>	***<u>72%</u>***	***<u>76%</u>***		
No fit assigned	27%	24%		RX[2]

Notes: **Bolded** COR correspond to those with low strain indicated in Table 4. See Methods for discussion of COR category determination. Total percentages of lamellae with COR using the Griffiths et al. (2016) classification are 80% and 93% for the CT and Austrian samples, respectively. COR types are from Habler and Griffiths (2017). [1]Hwang et al. (2016) [2]Griffiths et al. (2016).

Table 4: *d-spacing* ratios of host-lamellae pairs

		Rutile[2]			Ilmenite[3]			Corundum[4]		
		{100}	{110}	(001)	$\{11\bar{2}0\}$	$\{10\bar{1}0\}$	(0001)	$\{11\bar{2}0\}$	$\{10\bar{1}0\}$	(0001)
Garnet[1] $\mathrm{Py_{25}Alm_{55}Gro_{20}}$	{100}	0.397	0.281	0.256	0.220	0.381	1.217	0.206	0.356	1.122
	{110}	0.561	0.397	0.361	0.311	**0.538**	1.721	0.291	**0.504**	1.587
	{111}	0.687	**0.486**	0.443	0.381	0.659	**2.108**	0.356	0.617	**1.943**
	{112}	0.972	0.687	0.626	**0.538**	0.933	2.981	**0.504**	0.872	2.748

		Fluorapatite[5]			Hydroxylapatite[5]			Chlorapatite[5]		
		$\{11\bar{2}0\}$	$\{10\bar{1}0\}$	(0001)	$\{11\bar{2}0\}$	$\{10\bar{1}0\}$	(0001)	$\{11\bar{2}0\}$	$\{10\bar{1}0\}$	(0001)
Garnet[1] $\mathrm{Py_{25}Alm_{55}Gro_{20}}$	{100}	0.413	0.715	0.595	0.407	0.705	0.594	0.413	0.715	0.589
	{110}	0.584	**1.011**	0.841	0.575	**0.997**	0.841	0.584	**1.011**	0.832
	{111}	0.715	1.238	**1.030**	0.705	1.221	**1.030**	0.715	1.238	**1.020**
	{112}	**0.991**	1.717	1.457	**0.997**	1.726	1.456	**1.011**	1.750	1.442

		Kamacite[6]		
		{100}	{110}	{111}
Taenite[6]	{100}	0.799	0.565	0.462
	{110}	1.131	0.799	0.653
	{111}	1.385	**0.979**	0.799
	{112}	1.959	1.385	1.131

Notes: Calculations used lattice parameters at room temperature. **Bolded** pairs correspond to COR reported in Tables 2 and 3 (see Results subsection "COR Prediction Methods"). Trigonal minerals were calculated with hexagonal unit cell parameters. [1]Thiéblot et al. 1998; [2]Meagher and Lager 1979; [3]Wechsler and Prewitt 1984; [4]Fiquet et al. 1999; [5]Brunet et al. 1999; [6]Ramsden and Cameron 1966.